

CHEYENNE MOUNTAIN LATE TIME SIMULATION RESULTS(U) NAVAL  
RESEARCH LAB WASHINGTON DC K HAIN ET AL 07 JUN 85  
NRL-MR-5565

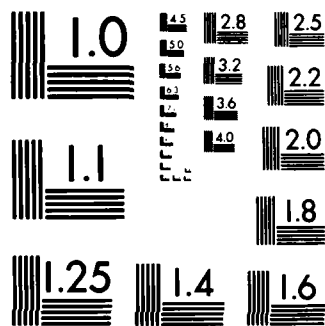
RESEARCH LAB WASHINGTON DC K HAIN ET AL 07 JUN 85  
NRL-MR-5565

F/G 18/3

NL

END

**Keywords:** child sexual abuse; disclosure; help-seeking; mental health



MICROCOPY RESOLUTION TEST CHART  
NATIONAL BUREAU OF STANDARDS-1963-A

(2)

NRL Memorandum Report 5565

AD-A155 425

## Cheyenne Mountain Late Time Simulation Results

K. HAIN, G. HAIN AND J. A. FEDDER

*Geophysical and Plasma Dynamics Branch  
Plasma Physics Division*

June 7, 1985

This research was sponsored by the Defense Nuclear Agency under Subtask S99QMXBC,  
work unit 00118 and work unit title "Late Time Electrostatic."



DTIC  
JUN 10 1985  
B

DTIC FILE COPY

NAVAL RESEARCH LABORATORY  
Washington, D.C.

Approved for public release; distribution unlimited

REPORT DOCUMENTATION PAGE				
1a REPORT SECURITY CLASSIFICATION <b>UNCLASSIFIED</b>		1b RESTRICTIVE MARKINGS		
2a SECURITY CLASSIFICATION AUTHORITY		3 DISTRIBUTION AVAILABILITY OF REPORT <b>Approved for public release; distribution unlimited.</b>		
2b DECLASSIFICATION/DOWNGRADING SCHEDULE		5 MONITORING ORGANIZATION REPORT NUMBER(S)		
4 PERFORMING ORGANIZATION REPORT NUMBER(S) <b>NRL Memorandum Report 5565</b>		7a NAME OF MONITORING ORGANIZATION		
6a NAME OF PERFORMING ORGANIZATION <b>Naval Research Laboratory</b>	6b OFFICE SYMBOL (if applicable) <b>Code 4780</b>	7b ADDRESS (City, State, and ZIP Code)		
6c ADDRESS (City, State, and ZIP Code) <b>Washington, DC 20375-5000</b>		9 PROCUREMENT INSTRUMENT IDENTIFICATION NUMBER		
8a NAME OF FUNDING/SPONSORING ORGANIZATION <b>Defense Nuclear Agency</b>	8b OFFICE SYMBOL (if applicable) <b>RAAE</b>	10 SOURCE OF FUNDING NUMBERS		
8c ADDRESS (City, State, and ZIP Code) <b>Washington, DC 20305</b>		PROGRAM ELEMENT NO. <b>62715H</b>	PROJECT NO.	TASK NO.
				WORK UNIT ACCESSION NO. <b>DN320-100</b>
11 TITLE (Include Security Classification) <b>Cheyenne Mountain Late Time Simulation Results</b>				
12 PERSONAL AUTHOR(S) <b>Hain, K., Hain, G. and Fedder, J.A.</b>				
13a TYPE OF REPORT <b>Interim</b>	13b TIME COVERED FROM <b>10/83</b> TO <b>9/84</b>	14 DATE OF REPORT (Year, Month, Day) <b>1985 June 7</b>	15. PAGE COUNT <b>56</b>	
16 SUPPLEMENTARY NOTATION <b>This research was sponsored by the Defense Nuclear Agency under Subtask S99QMXBC, work unit 00118 and work unit title "Late Time Electrostatic."</b>				
17 COSATI CODES		18 SUBJECT TERMS (Continue on reverse if necessary and identify by block number)		
FIELD	GROUP	SUB-GROUP		
		HANE		
		Nuclear weapons phenomenology; Nuclear simulation; Late-time electrostatic		
19 ABSTRACT (Continue on reverse if necessary and identify by block number)  In this report we present results for the late time evolution of the Cheyenne Mountain nuclear explosion scenario. Results are presented from both the DEMAG simulation code and the MELT simulation code. The results are compared and the differences between them are explained. We conclude that the simulation results are in good agreement.				
20 DISTRIBUTION AVAILABILITY OF ABSTRACT <input checked="" type="checkbox"/> UNCLASSIFIED UNLIMITED <input type="checkbox"/> SAME AS RPT <input type="checkbox"/> OTIC USERS		21 ABSTRACT SECURITY CLASSIFICATION <b>UNCLASSIFIED</b>		
22a NAME OF RESPONSIBLE INDIVIDUAL <b>J. D. Huba</b>		22b TELEPHONE (Include Area Code) <b>(202) 767-3630</b>		22c OFFICE SYMBOL <b>Code 4780</b>

## CONTENTS

I. INTRODUCTION .....	1
II. CODE DESCRIPTION .....	2
III. RESULTS .....	4
IV. DISCUSSION .....	7
ACKNOWLEDGMENT .....	10
APPENDIX A .....	11
APPENDIX B .....	13
APPENDIX C .....	16
REFERENCES .....	44

DTIC  
ELECTE  
JUN 26 1985  
B



Accession	✓
NTIS	
DTIC	
DATE	
BY	
REMARKS	
A-1	

## CHEYENNE MOUNTAIN LATE TIME SIMULATION RESULTS

### I. INTRODUCTION

The Cheyenne Mountain nuclear detonation scenario involved a high altitude ( $> 150$  km), large yield ( $> 1$  M ton) nuclear explosion over the central Rocky Mountain region of the U.S. Such high altitude nuclear explosions (HANE) evolve through a number of temporal stages during which the physical description of the explosion and the effects are radically different from each other. For the simulation results presented in this report we are concerned with the last and longest period of evolution of a HANE; a period, hours in length, when the vast amount of plasma created in the explosion slowly evolves, and the ionosphere and magnetosphere return to their pre-burst condition.

The computer codes which have been developed to study the period are commonly termed "late-time electrostatic codes". There are two of these codes: the NRL code DEMAG and the MRC code MELT. The codes are "late time" because they simulate HANE phenomenology later than about 5 min after detonation. They are termed "electrostatic" because plasma motion perpendicular to the geomagnetic field is treated in terms of an electrostatic potential field. The theory for the perpendicular plasma transport for the DEMAG code has been reported in Hain and Fedder (1984). The theory for the parallel plasma transport is the usual hydrodynamic theory. The theory for the MELT code has been previously reported in Longmire and Kilb (1977) and Kilb (1977).

In this report we will discuss and compare the two codes DEMAG and MELT which use very different algorithms. We will show results of simulations from each code for the Cheyenne Mountain scenario during the

Manuscript approved February 25, 1985.

temporal period of 5 to 30 minutes after burst. We will discuss the results pointing out similarities and differences between them. Finally we will briefly summarize these results and present our conclusions.

## II. CODE DESCRIPTION

Although both codes, DEMAG and MELT, are designed to solve an identical set of theoretical equations, the numerical algorithms used are considerably different. The DEMAG numerical algorithm used for both neutral atmosphere and plasma transport is an "Eulerian" algorithm; the numerical grid is a constant fixed mesh. Both the plasma and the neutral gas are transported across the grid from mesh point to mesh point. The MELT code uses a "Lagrangian" algorithm for the plasma transport. That is, as plasma is transported from point to point in space, the numerical mesh points are moved along with the plasma and the same parcel of plasma remains within the same numerical cell. The neutral atmosphere in the MELT code uses a fixed "Eulerian" mesh as does the DEMAG code.

Figures 1 and 2 show the DEMAG fixed meshes for the plasma and the neutral gas, respectively, on a geomagnetic meridional plane in the Northern hemisphere. For the plasma (Fig. 1) the coordinate lines are magnetic field lines and magnetic potential lines. For the neutral gas (Fig. 2) the coordinate lines are an adapted coordinate system which tends toward a magnetic orientation at high altitudes and is spherical at low altitudes; the coordinate system is described mathematically in Appendix A. In each case the third coordinate is the rotational coordinate about the magnetic axis. Figure 3 is a similar diagram to Fig. 1 except it shows the MELT plasma mesh. Here one can clearly see the magnetic field line coordinate but the coordinate along the field is unequally spaced and is controlled by the motion of plasma along the field line. The MELT neutral

atmosphere mesh is an earth centered spherical mesh which terminates at 1500 km altitude and is not shown here.

The choice of numerical meshes for the simulations is controlled by a number of considerations. The spherical nature of the neutral atmosphere at low altitudes is required to allow the burst disrupted atmosphere to return to a sensible hydrostatic equilibrium. The distortion of the DEMAG neutral mesh at higher altitudes towards a geomagnetic mesh is designed to allow a better description of neutral gas motion as it is carried to high altitudes by the plasma.

Both codes, DEMAG and MELT, make use of a geomagnetic field aligned mesh for the plasma owing to consideration of the electrostatic nature of the plasma transport at late times. For electrostatic plasma transport the magnetic field is considered to be constant. Moreover, plasma motion perpendicular to the field has a very special property; specifically, all plasma on a common field line (more correctly contained in a common flux tube) at a particular moment of time remains on a common field line (in a common flux tube) for all time. The plasma is said to be "frozen" to the field. A geomagnetic field line coordinate therefore is a natural choice for the plasma mesh.

The DEMAG choice of "Eulerian" transport on the geomagnetic mesh involved two considerations. First, it was felt that modern numerical methods were sufficiently accurate to adequately control numerical errors and to maintain a good approximation to the field frozen plasma motion described above. Second, Eulerian transport is inherently simpler in multiple dimensions because of the fixed numerical grid, and in such large codes, simplicity is an advantage where obtainable. The MELT code has the advantage that the Lagrangian transport exactly satisfies the field frozen plasma motion until the numerical grid becomes too distorted for further



computation. At this point the grid must be restructured which is a complex and difficult operation, and to some undetermined extent violates the field frozen condition thereby partially negating its initial advantage.

Clearly there are many possible choices to be made when developing simulation codes as complex and difficult as DEMAG and MELT. Different people will make different choices and all for good reasons. It is therefore not too surprising that two very different codes have been developed to simulate the same types of HANE problems. The quality of the codes and the different approaches can only be tested by comparing simulation results to data. In the absence of hard data, which is almost non-existent for late time HANE, the quality of simulations can only be verified by comparing results from different codes. In the case of two very different codes such as DEMAG and MELT such a comparison of results can provide a verity to the results which would otherwise be totally unattainable.

### III. RESULTS

In this report we show results from both the DEMAG and MELT simulations for the Cheyenne Mountain HANE scenario for the time period 300 to 1800 seconds after burst. The two simulation codes were initialized at 300 seconds with the same data set which was generated by MRC with the MICE MHD nuclear simulation code.

At 300 sec the initial blast wave from the burst has propagated far from the burst point. The large cavity in the geomagnetic field has collapsed and the magnetic field has returned to ambient values. The remnant of the HANE is a large, geomagnetic field aligned plume of plasma which extends from the northern conjugate to the southern conjugate

ionosphere. The lower portion of this plasma plume with plasma densities greater than  $10^8 \text{ cm}^{-3}$  is shown in Figs. 4 and 5. The plasma in the plume is moving at high velocities along the field lines in order to achieve a hydrostatic equilibrium and at lower altitudes in response to strong upward neutral atmospheric heave winds. The still highly disturbed neutral atmospheric densities are shown in Figs. 6 and 7. The geomagnetic field lines which contain the plasma plume pass through the equatorial plane of the magnetosphere at altitudes above one earth radius. Figure 8 which shows a contour diagram of the field line integrated densities at the geomagnetic equator shows the great size of the plasma plume at high altitudes. It is more than 2000 km in width and 4000 km in depth perpendicular to the geomagnetic field.

During the simulation the plasma in the geomagnetic field aligned plume evolves. It loses density via recombination at low altitudes in the ionosphere. The plasma moves up and down along the field lines in response to pressure and gravity forces, and also in response to the neutral atmosphere heave winds. Motion of the plume perpendicular to the geomagnetic field occurs due to gravity forces, centrifugal forces, coriolis forces, and neutral wind friction forces. The motions along the field and recombination slowly deplete the plume plasma density, while motions perpendicular to the field distort and stretch the plume onto higher latitude flux tubes or compress the plume onto lower latitude flux tubes. The plume can also drift slowly relative to the earth's rotation.

The cumulative effects of these processes on the plasma plume can be seen in Figs. 9-11 while the relaxation of the neutral atmosphere to near ambient density is seen in Fig. 12. In studying the plasma density in Figs. 9 and 10 it is noted that the maximum plasma density in the plume has

fallen by about a factor of 3 in one half hour. The plume has moved poleward (northern plume northward - southern plume southward) about 600 km. Moreover, the poleward border of the plasma plume is more diffuse and has a considerably reduced density gradient. A better picture of the poleward motion can be seen by comparing the result in Fig. 11 with the initialization in Fig. 8. In this comparison it is seen that the eastward and westward portions of the plume plasma has remained almost stationary while the center has moved upward in the equatorial plane. The motion in the ionosphere is similar. The eastward and westward portion of the plumes remain almost stationary while the center of the plume moves poleward. A comparison of Figs. 9-11 shows that the field frozen plasma motion results in higher velocities at high altitudes. As the plume moves 600 km poleward in the ionosphere the equatorial portion of the plume moves 3000 km higher.

Figures 13 and 14 show MELT results for the plasma density at 1800 secs; they are to be compared to Figs. 9 and 10 of the DEMAG results. One first notices that the maximum plasma densities in the two sets of results are very nearly the same, and that both plasma plumes appear to be decaying in a similar manner. There are, however, some differences. The poleward density gradient in the MELT results is much sharper than in DEMAG. This difference could be a result of the different numerical algorithms, that is, a result of the Eulerian algorithm in DEMAG allowing more diffusion across the geomagnetic field; or it could be the result of the more evolved poleward plume motion in DEMAG. The DEMAG plasma plume moves about twice as far poleward as does the plume in the MELT simulation. The difference in poleward motion of the two plumes will be discussed more fully later as it appears to be the major difference between the simulation results.

Comparisons between the results of the simulations for other plasma and atmospheric properties can be carried out by using the microfiche. The fiche contain plasma and neutral densities, pressure, and temperature; species densities; and plasma and neutral motions. The DEMAG results are shown starting with initial conditions at 300 sec intervals between 300 and 1800 sec. The MELT results are shown at 600 sec intervals between 600 and 1800 secs. A description of the fiche figures and layout is contained in Appendix B.

#### IV. DISCUSSION

The DEMAG and MELT results shown on the fiche have been compared to each other between 600 and 1800 sec. The comparison of data shows an overall agreement between results, particularly if one is interested in the high plasma density regions of the plume. Results for plasma and neutral densities, temperatures and species densities are all very similar and are approximately equal. The primary difference between the results involves the poleward and upward motion of the plume. The DEMAG plume moves faster and about twice as far poleward as the MELT plume. We think this difference in motion perpendicular to the geomagnetic field has a straightforward explanation which follows.

In both DEMAG and MELT the primary forces driving plasma motion perpendicular to the geomagnetic field are neutral drag, caused by atmospheric heave and relaxation; centrifugal forces, caused by rapid plasma motion along the curved geomagnetic field in the plume; and gravitational attraction, pulling the plasma plume downward and equatorward. For the Cheyenne Mountain simulation these three forces are initially in a very sensitive balance: the neutral drag and centrifugal

forces pushing upward, and gravity pulling downward. If either of the codes emphasizes or diminishes one of these forces relative to the other code, we would expect a difference in motion owing to alterations in the sensitive balance of the driving forces.

Figures 15 and 16 show potential plots for DEMAG and MELT, respectively, at 600 secs. Plasma flow is along the potential contours perpendicular to the geomagnetic field. The potential contours are shown on the geomagnetic equatorial plane. The reader will notice immediately that the contours near the boundaries in the two figures are decidedly different. The difference arises due to different boundary conditions for DEMAG and MELT but are not significant to the results since motion in these regions involves only incompressible flow of almost uniform ambient background ionosphere. Near the center of the plots the flow lines are much more similar.

The DEMAG results (Fig. 15) show three different regions of flow in the plasma plume. Between 6000 and 8000 km altitude there is strong upward flow near the center plane of the plume. The upward flow turns outward and then downward near the edges of the plume. This region of flow is driven by a local dominance of the centrifugal force term. At higher altitudes between 9,000 and 11,000 km the flow throughout the central portion of the plume is downward. This downward flow region is driven by a local dominance of the gravitational force term. Finally, in the highest portion of the plume, between 11,000 and 14,000 km, the flow near the central plane is again upward and is controlled by a local dominance of the neutral drag force term. (The neutral drag does not occur at these equatorial altitudes but takes place at the poleward border of the plume at lower altitudes.)

Similar flow features can be seen in the MELT results (Fig. 16). The low altitude upward flow occurs between 5500 and 7500 km altitudes. The downward flow occurs throughout the central portion of the plume between 8000 and 11,000 km. Above 11,000 km the downward flow is substantially weakened, where the DEMAG results show upward flow. These results can possibly be seen more clearly in the velocity vector diagrams shown in Figs. 17 and 18 for DEMAG and MELT, respectively.

The primary areas of disagreement in these results relate to the absence of upward flows at the highest altitudes in the MELT results and to the faster downward flow in the central plume shown in the MELT results relative to those of DEMAG. The reason for these differences is shown in Figs. 19-22.

Figures 19 and 20 show the neutral atmospheric densities on the central meridional plane at 600 sec for both the northern and southern conjugate regions. Of particular interest is the large atmospheric density above 1500 km altitude (the top of the MELT neutral grid) which occurs in both hemispheres. The high neutral density, because of its great extent along the geomagnetic field, can be very effective in enhancing the neutral drag force term in DEMAG relative to that in MELT. Figures 21 and 22 show that the neutral velocities at these high altitudes are primarily upward and poleward relative to the geomagnetic field, and therefore the enhanced neutral drag force term would strengthen upward and poleward plume motion. Since this force occurs at altitudes above 1500 km the MELT results do not account for it and therefore the MELT plume experiences less poleward acceleration. Increasing the MELT neutral atmospheric grid to roughly double its present height would be expected to bring the results into much closer agreement.

At 1800 secs, Figs. 23 and 24 show potential contours and Figs. 25 and 26 show velocity vectors for DEMAG and MELT, respectively. At this late time the plasma plumes in both results are moving primarily upward and poleward. The DEMAG plasma which began moving poleward earlier and more strongly continues to move slightly faster. This continuing difference in the results can again be traced back to the more dominant neutral drag force than in the DEMAG simulation at earlier times. At this time, the centrifugal force term is dominant and is forcing the upward and poleward motion. As the plasma motion in the plume parallel to the geomagnetic field slows and relaxes, gravitational forces will eventually dominate and will then cause the plume to fall and move equatorward. Since the DEMAG plume moves further poleward the DEMAG results indicate a more lengthy return to equilibrium than do the MELT results. More complete analysis of the complex perpendicular motion and the delicate balance of forces can be undertaken by study of the fiche entitled "POT". The fiche show potentials, velocities and force terms for the DEMAG simulations. The "POT" fiche are described in Appendix C.

In summary, we would conclude that the DEMAG and MELT simulations of the Cheyenne Mountain scenario are in good agreement. The primary disagreement involving perpendicular motion is understood and has been explained. We have also discussed the implications of that disagreement for later time evolution of the plasma plume. Both codes DEMAG and MELT appear to provide reasonably accurate results for the late time evolution of a high altitude nuclear explosion.

#### ACKNOWLEDGMENT

This research has been supported by the Defense Nuclear Agency.

## Appendix A

This appendix discusses the derivation of the NRL DEMAG coordinate system for the neutral atmosphere. For reasons discussed in the text, this coordinate systems tends to dipolar magnetic coordinates at high altitudes and tends to a spherical coordinate system at low altitudes.

We consider a function of  $f(y, r, \theta) = 0$  where  $y$  is a coordinate line description,  $r$  is the geocentric radius normalized to the earth radius and  $\theta$  is the geomagnetic colatitude. Moreover, we require  $f$  to be a monotone function of  $r$  and  $\theta$ , for  $\eta$  positive. The unit vectors perpendicular to  $\eta$  are given by

$$e_r = \frac{\partial f}{\partial r} / \sqrt{(\partial f / \partial r)^2 + (1/r \partial f / \partial \theta)^2}$$

$$e_\theta = \frac{1}{r} \frac{\partial f}{\partial \theta} / \sqrt{(\partial f / \partial r)^2 + (1/r \partial f / \partial \theta)^2}.$$

We now require that

$$e_r = 0 \text{ at } r = 1 \text{ (earths surface)}$$

$$e_\theta = 0 \text{ at } \theta = \frac{\pi}{2} \text{ (magnetic equator)}$$

A simple function which satisfies these conditions is

$$f = \frac{(r - 1)^\epsilon}{(\eta - 1)^{\epsilon-1}} - (\eta \sin^2 \theta - 1) \text{ for } \epsilon > 1.$$



For  $\epsilon = 1$ ,  $f$  describes a dipolar coordinate line; whereas for  $\epsilon = \infty$ ,  $f$  describes a radial coordinate line. For the DEMAG neutral mesh, we use  $\epsilon = 2$ .

To numerically generate the grid we construct a coordinate line through the burst point and compute its total length. We subdivide this coordinate line to obtain one set of coordinates and then construct an orthogonal mesh to each side of this base coordinate line. The resulting mesh is displayed in figure 2.

The neutral boundary conditions are reflecting at 100 km altitude and out-flow on the other boundaries.

## Appendix B

Tables B1 and B2 show the layout of the plots on the microfiche for the DEMAG and MELT results, respectively. The NRL fiche show the DEMAG results at 300 sec intervals between 300 and 1800 sec. The MRC fiche show the MELT results at 600 sec intervals between 600 and 1800 sec.

The quantities  $N_e$ ,  $v_{\perp}$ , and  $\Psi$  are the field line integrated density, the perpendicular to B velocity and the electrostatic potential, respectively, plotted on the geomagnetic equatorial plane.  $n$ ,  $P$ , and  $T$  are the density, pressure, and temperature, respectively. (N), (S), and (V) indicate the northern conjugate, southern conjugate meridional plane, and a vertical plane 5300 km north of the equator through the burst region and perpendicular to the central meridional plane. Subscripts e, p, i, N and v indicate electrons, plasma, ions, neutrals, and  $N_2$  vibrational state, respectively.

Individual constituents enclosed in brackets, such as  $[N^+]$  indicate species concentrations. A arrow,  $\rightarrow$ , designates a vector plot and a star,  $*$ , signifies an expanded view of the burst and conjugate regions. A double star,  $**$ , indicates a unit vector plot to show flow directions. For the vertical plane velocities,  $v_x$ ,  $v_y$ , and  $v_z$  show velocities in the meridional, longitudinal and vertical direction, respectively. For the MRC fiche a parallel,  $\parallel$ , designates velocities parallel to the magnetic field.

All quantities are plotted in cgs units.

Table B1--NRL CHEYENNE

Title	$n_e(S)$	$T_e(N)$	$[O_2^+](S)$	$n_N^*(S)$	$T_n(S)$	$[N_2](N)$	$\vec{v}_n^{**}(N)$	$v_y(V)$
	$n_e^*(S)$	$T_i(S)$	$[O_2^+](N)$	$n_N^*(N)$	$T_v(N)$	$[O_2](S)$	$ v_N $	$v_z(V)$
Plasma grid	$n_e^*(N)$	$T_i(N)$	$[NO^+](S)$	$n_N(N)$	$[N](S)$	$[O_2](N)$	$n_N(V)$	$ v_N (V)$
	$n_e(N)$	$[N^+](S)$	$[NO^+](N)$	$P_N(S)$	$[N](N)$	$[NO](S)$	$P_N(V)$	$\vec{v}_N(V)$
$N_e$	$P_p(S)$	$[N^+](N)$	$v_p(S)$	$P_N(N)$	$[O](S)$	$[NO](N)$	$T_N(V)$	
$\vec{v}_1$	$P_p(N)$	$[O^+](S)$	$\vec{v}_p(N)$	$T_N(S)$	$[O](N)$	$\vec{v}_n(S)$	$T_v(V)$	
$\Psi$	$T_e(S)$	$[O^+](N)$	$n_N(S)$	$T_N(N)$	$[N_2](S)$	$\vec{v}_n(N)$	$v_x(V)$	

Table B2--MRC CHEYENNE

	$n_e(S)$	$T_e(N)$	$[NO](S)$	$n_N^*(S)$	$T_v(S)$	$[N_2](N)$	$\vec{v}_n^{**}(N)$	$v_y(V)$
Title	$n_e^*(S)$	$T_i(S)$	$[NO^+](N)$	$n_N^*(N)$	$T_v(N)$	$[O_2](S)$	$ v_N $	$v_z(V)$
Plasma grid	$n_e^*(N)$	$T_i(N)$	$[H^+](S)$	$n_N(N)$	$[N](S)$	$[O_2](N)$	$n_N(V)$	$ v_N (V)$
Neutral grid	$n_e(N)$	$[N^+](S)$	$[H^+](N)$	$P_N(S)$	$[N](N)$	$[NO](S)$	$P_N(V)$	$\vec{v}_N(V)$
$N_e$	$P_p(S)$	$[N^+](N)$	$v_p^I(S)$	$P_N(N)$	$[O](S)$	$[NO](N)$	$T_N(V)$	
$\vec{v}_1$	$P_p(N)$	$[O^+](S)$	$v_p^I(N)$	$T_N(S)$	$[O](N)$	$\vec{v}_n(S)$	$T_v(V)$	
$\Psi$	$T_e(S)$	$[O^+](N)$	$n_N(S)$	$T_N(N)$	$[N_2](S)$	$\vec{v}_n(N)$	$v_x(V)$	

## Appendix C

The POT fiche show quantities related to the electrostatic potential equation. The organization of the fiche are shown in Table C1. The quantities presented are field line integrated and are shown on the geomagnetic equatorial plane. Various quantities are described by a series of letters which indicate their identity. First letters D, T, and F signify ion-neutral drag or friction forces; transport forces including the convective derivative, coriolis forces, and centrifugal forces; and body forces including the pressure gradient and gravity, respectively. The second letters P and H indicate Pedersen and Hall components, respectively. The subscripts 1 and 2 indicate the meridional and longitudinal components, respectively. The sum of the forces are signified by S1 and S2 where  $S1 = DP2 + TP2 + FP2 + DH1 + TH1 + FH1$  and  $S2 = DP1 + TP1 + FP1 + DH2 + TH2 + FH2$ . The symbol R shows the divergence of S. The symbols C and E signify the capacitance and conductivity matrices, respectively, with the subscripts indicating which matrix element.

The theory and derivations for the quantities in the POT fiche are fully described in Hain and Fedder (1984).

Table C1—NRL POT CHEY

	DP <sub>2</sub>	TH <sub>2</sub>	C <sub>11</sub>
Title	TP <sub>2</sub>	FH <sub>2</sub>	C <sub>22</sub>
$\psi$	FP <sub>2</sub>	S <sub>1</sub>	C <sub>12</sub>
$\vec{v}_1$	DH <sub>1</sub>	S <sub>2</sub>	E <sub>11</sub>
DP <sub>1</sub>	TH <sub>1</sub>	$v_1 S_1$	E <sub>22</sub>
TP <sub>1</sub>	FH <sub>1</sub>	$v_2 S_2$	E <sub>12</sub>
FP <sub>1</sub>	DH <sub>2</sub>	R	

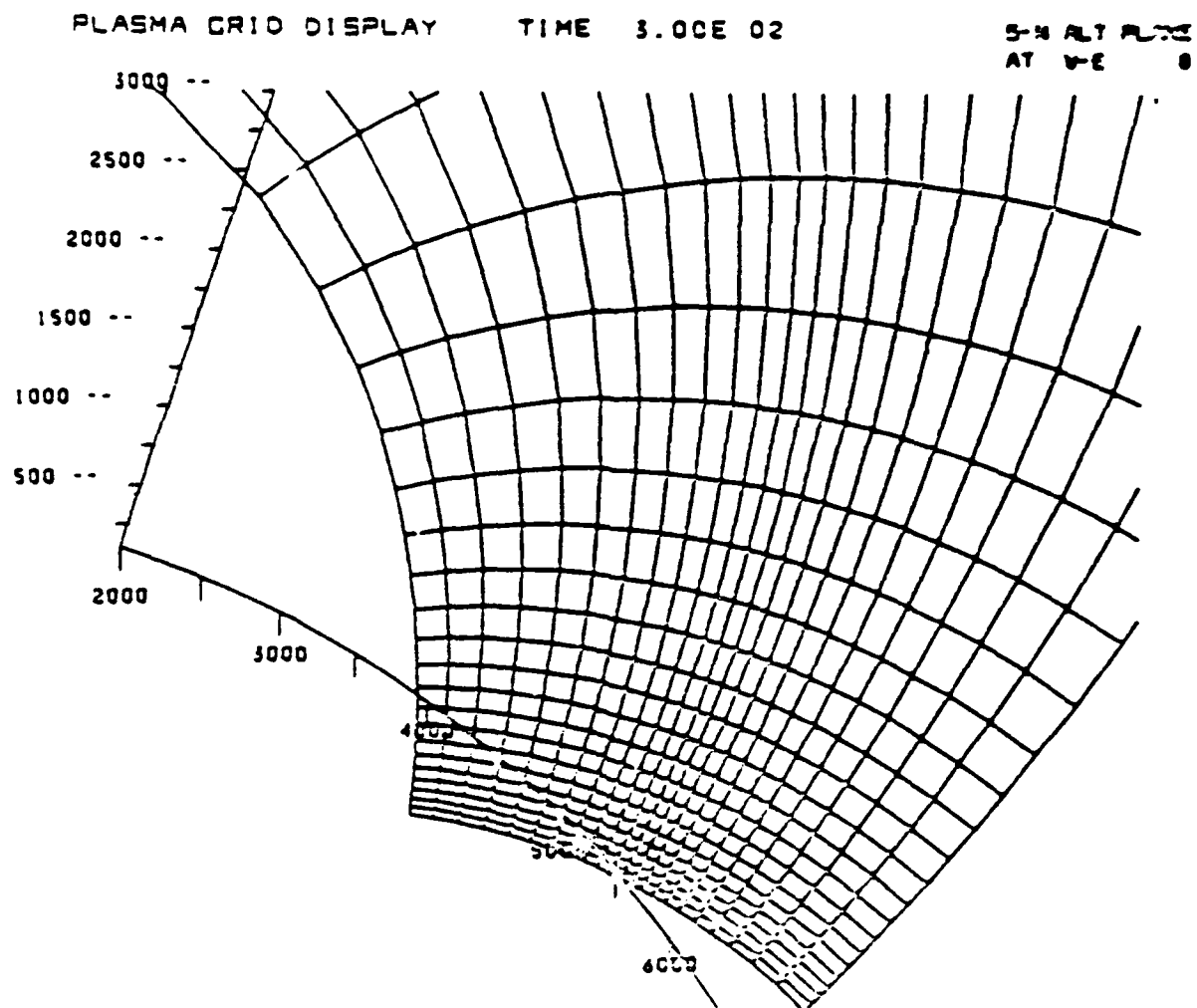


Figure 1. A plot of the geomagnetic field aligned plasma grid for the DEMAG code on a meridional plane in the northern conjugate region. The vertical scale is altitude and the horizontal scale is distance from the geomagnetic equator along the earth's surface in kilometers.

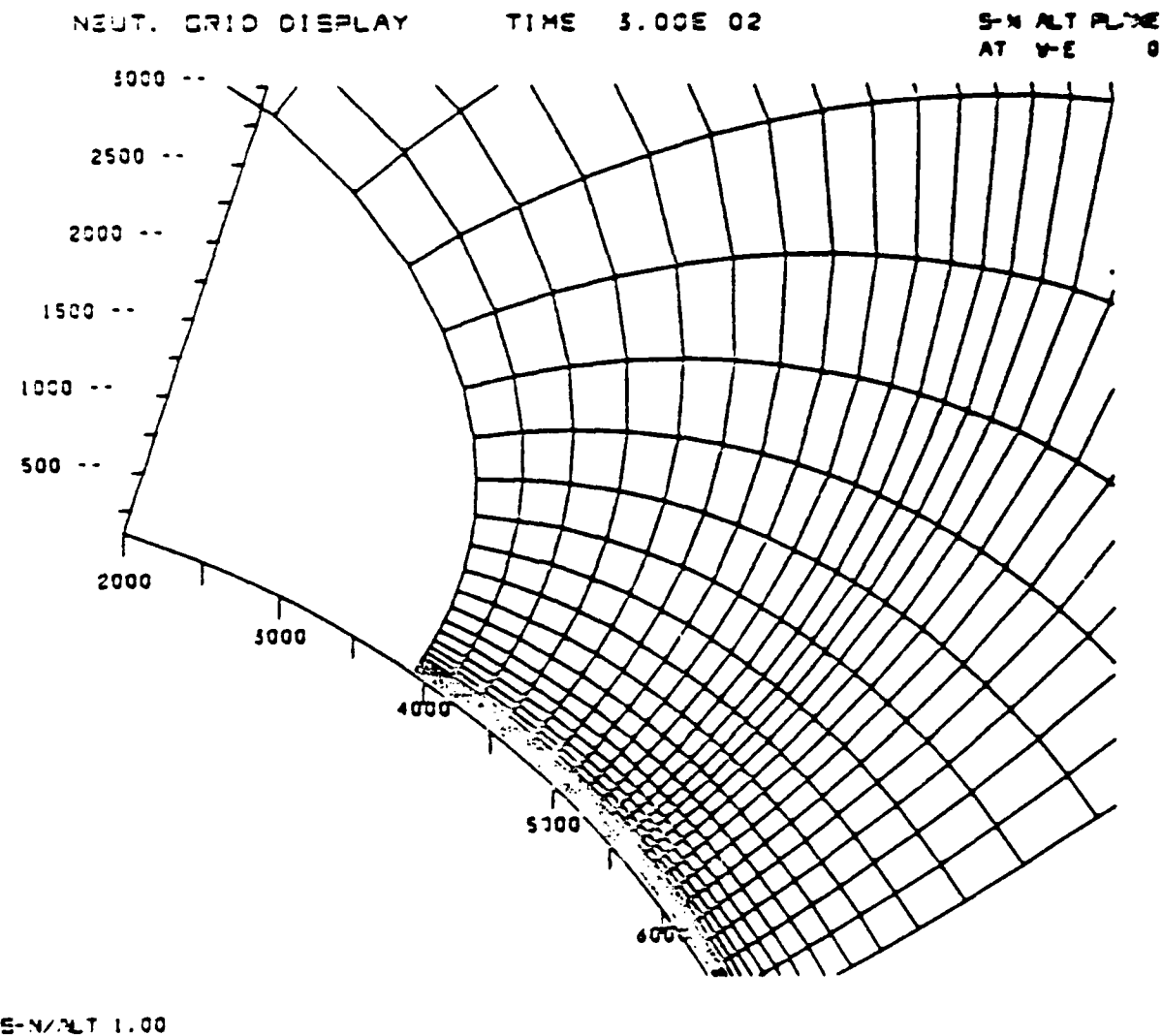


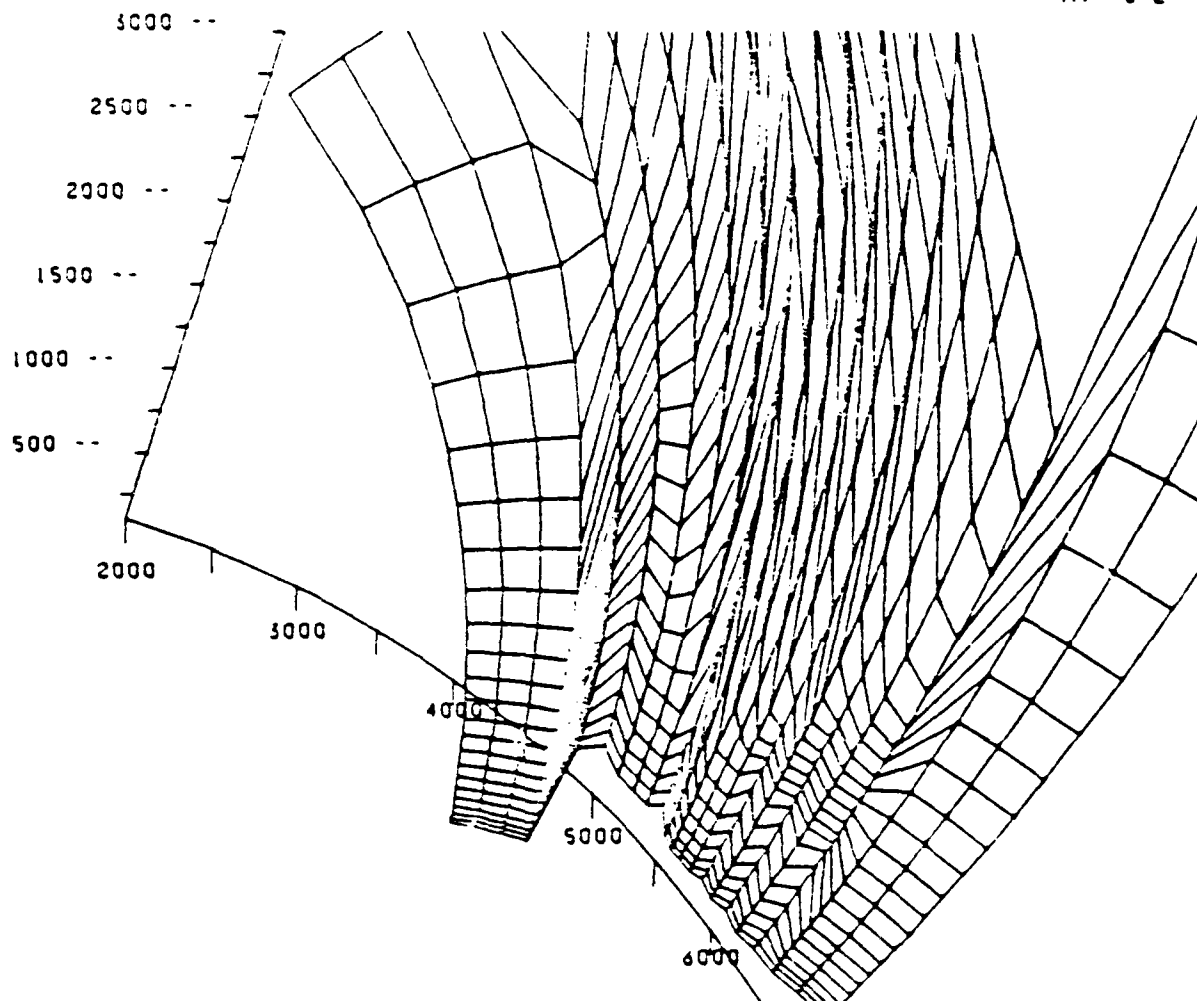
Figure 2. A plot of the neutral atmosphere grid for the DEMAG code on a meridional plane in the northern conjugate region. The vertical and horizontal scales are identical to those in Figure 1.



PLASMA GRID DISPLAY

TIME 1.80E 03

S-N ALT PLANE  
AT V-E 0



S-N/ALT 1.00

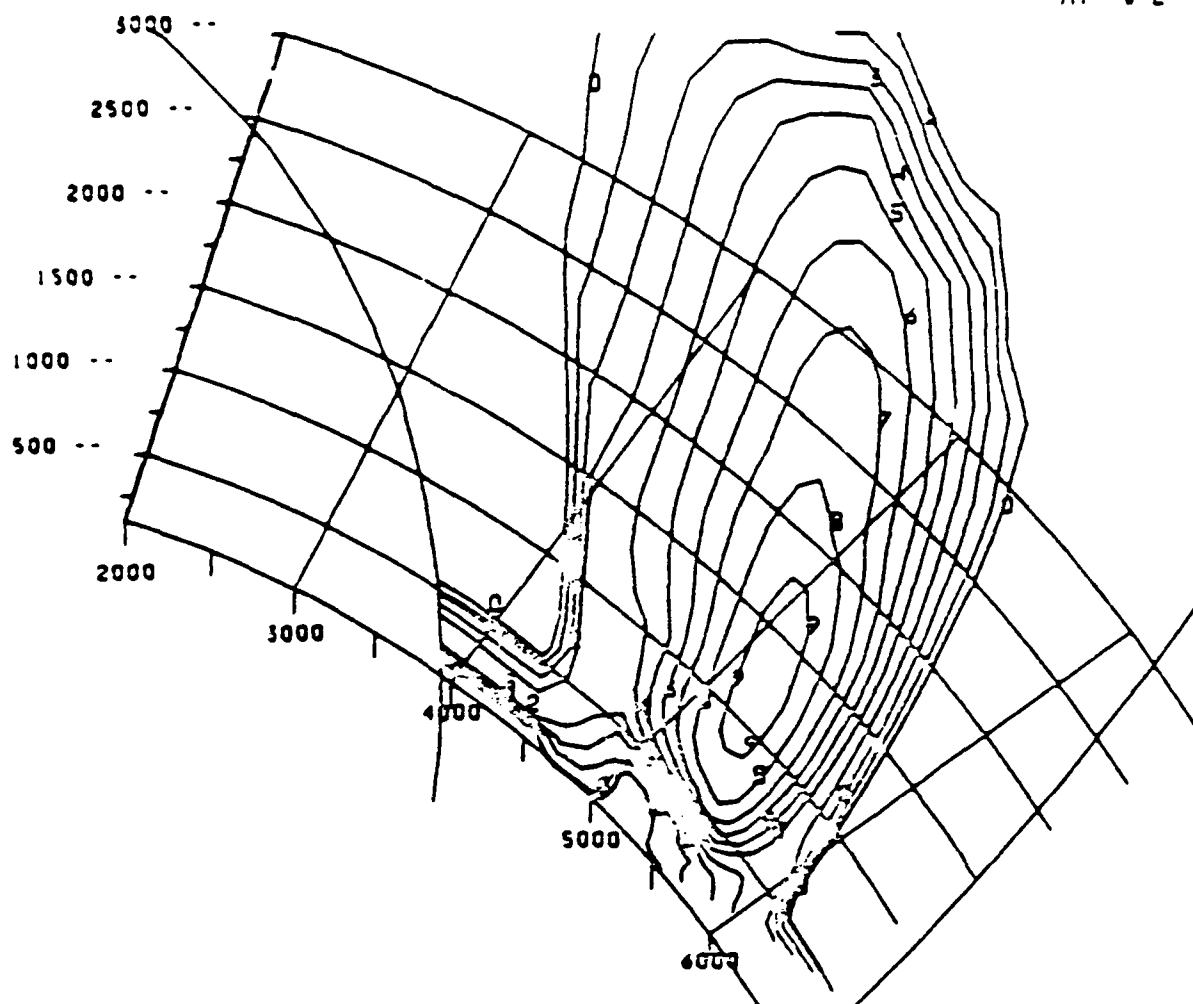
MCEV

Figure 3. A plot of the "Lagrangian" geomagnetic field aligned plasma grid for the MELT code on a meridional plane in the northern conjugate. The vertical and horizontal scales are identical to those in Figure 1.

NE AT PHI=0

TIME 3.00E 02

S-N ALT PLANE  
AT V-E 0



S-N/ALT 1.00

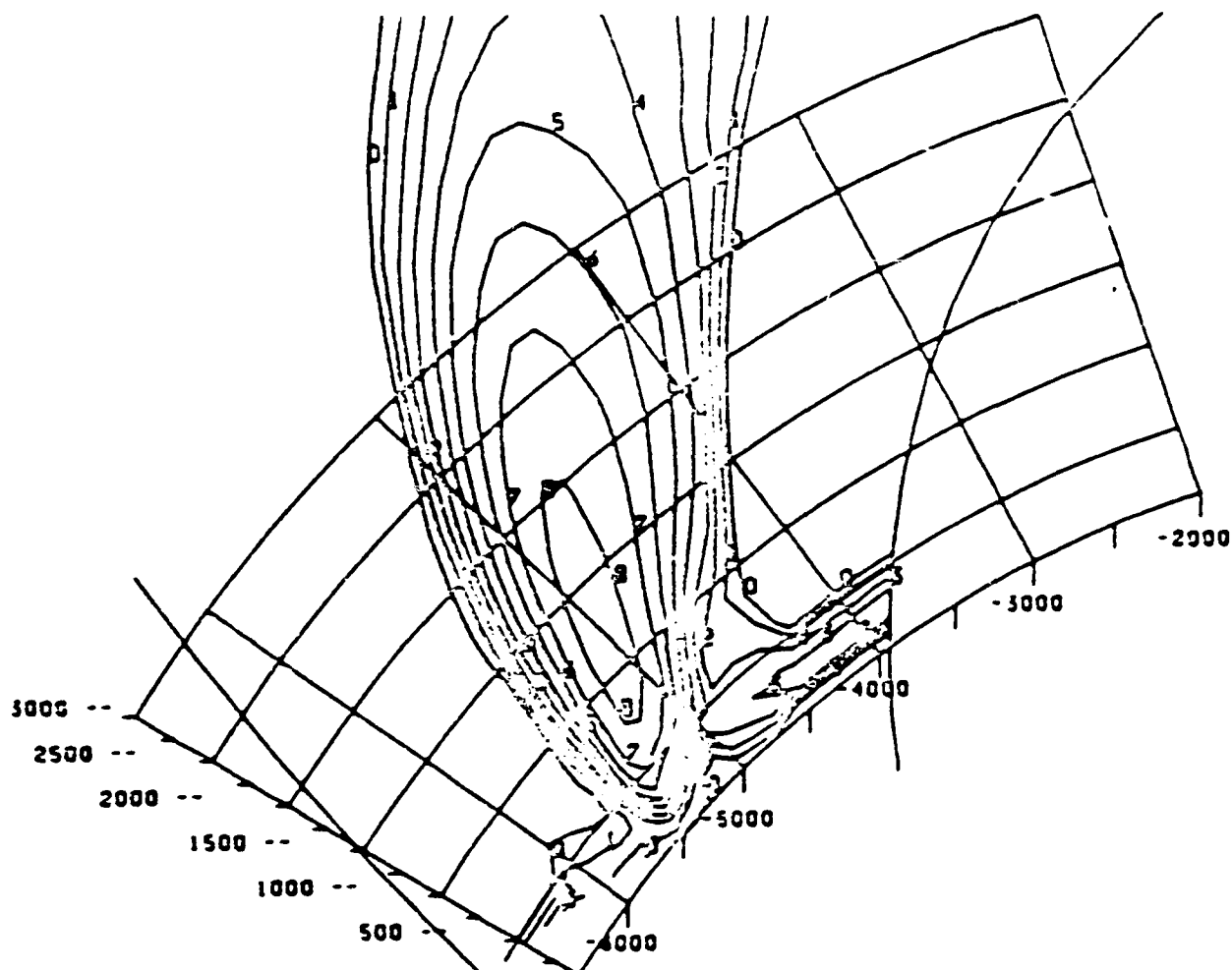
0. 1.0E 04    1. 3.0E 04    2. 1.0E 05    3. 3.0E 05    4. 1.0E 06  
5. 3.0E 06    6. 1.0E 07    7. 3.0E 07    8. 1.0E 08    9. 3.0E 08    10. 1.0E 09    11. 3.0E 09    12. 1.0E 10    13. 3.0E 10    14. 1.0E 11

Figure 4. A contour plot of initial condition electron densities at 300 seconds on the northern conjugate central, meridian plane. Contour levels in electrons  $\text{cm}^{-3}$  are shown at the bottom of the graph.

NE AT PHI=0

TIME 3.01E 03

3-1 ALT PLANE  
AT V-E 0



S-N/ALT 1.00

0 • 1.0E 04	1 • 3.0E 04	2 • 1.0E 05	3 • 3.0E 05	4 • 1.0E 06
5 • 3.0E 06	6 • 1.0E 07	7 • 3.0E 07	8 • 1.0E 08	

NLCY

Figure 5. A contour plot of initial condition electron densities at 300 seconds on the southern conjugate central meridional plane. Contour levels in electrons  $\text{cm}^{-3}$  are shown at the bottom of the graph.

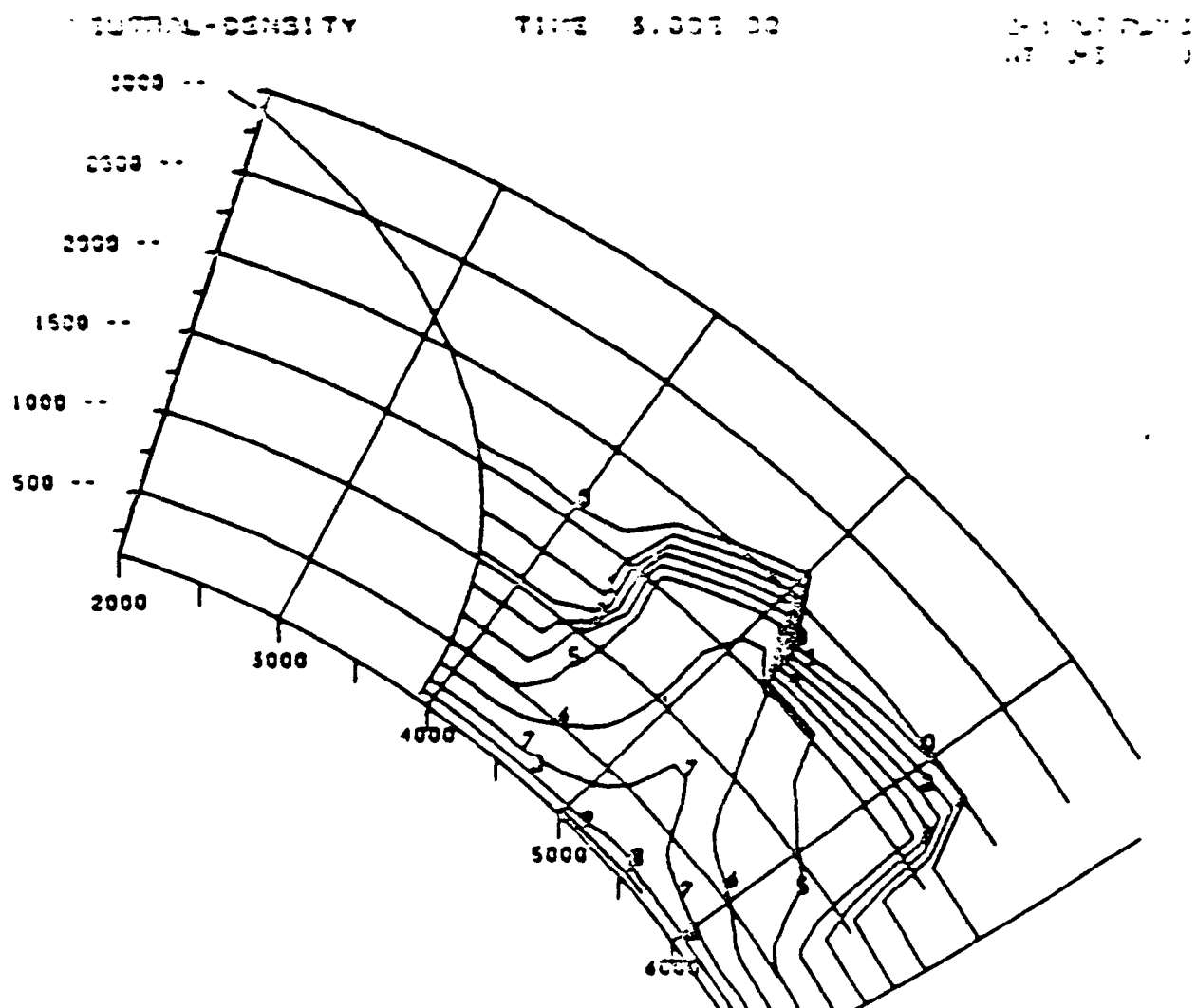
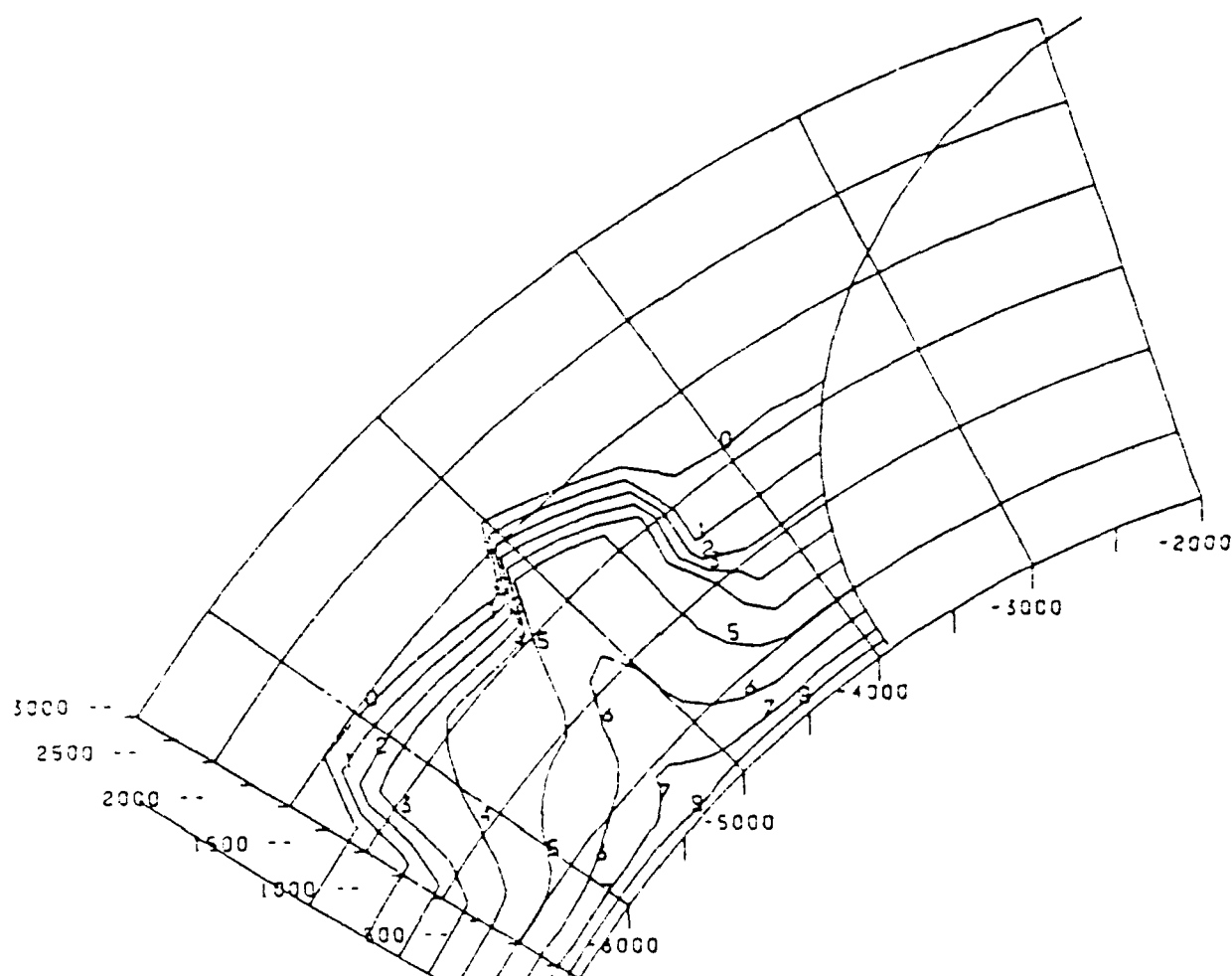


Figure 6. A contour plot of initial conditions neutral atmospheric density at 300 seconds on the northern conjugate central meridian plane. Contour levels are shown in gauss  $\text{cm}^{-3}$  at the bottom of the graph. The sharp cutoff in atmospheric density above 1500 kilometers altitude is caused by the termination of the MICE/MELT neutral atmosphere numerical mesh.

NEUTRAL-DENSITY

TIME 3.00E 02

S-N ALT PLANE  
AT V-E 0

0 • 1.0E-20    1 • 1.0E-19    2 • 1.0E-18    3 • 1.0E-17    4 • 1.0E-16

5 • 1.0E-15    6 • 1.0E-14    7 • 1.0E-13    8 • 1.0E-12

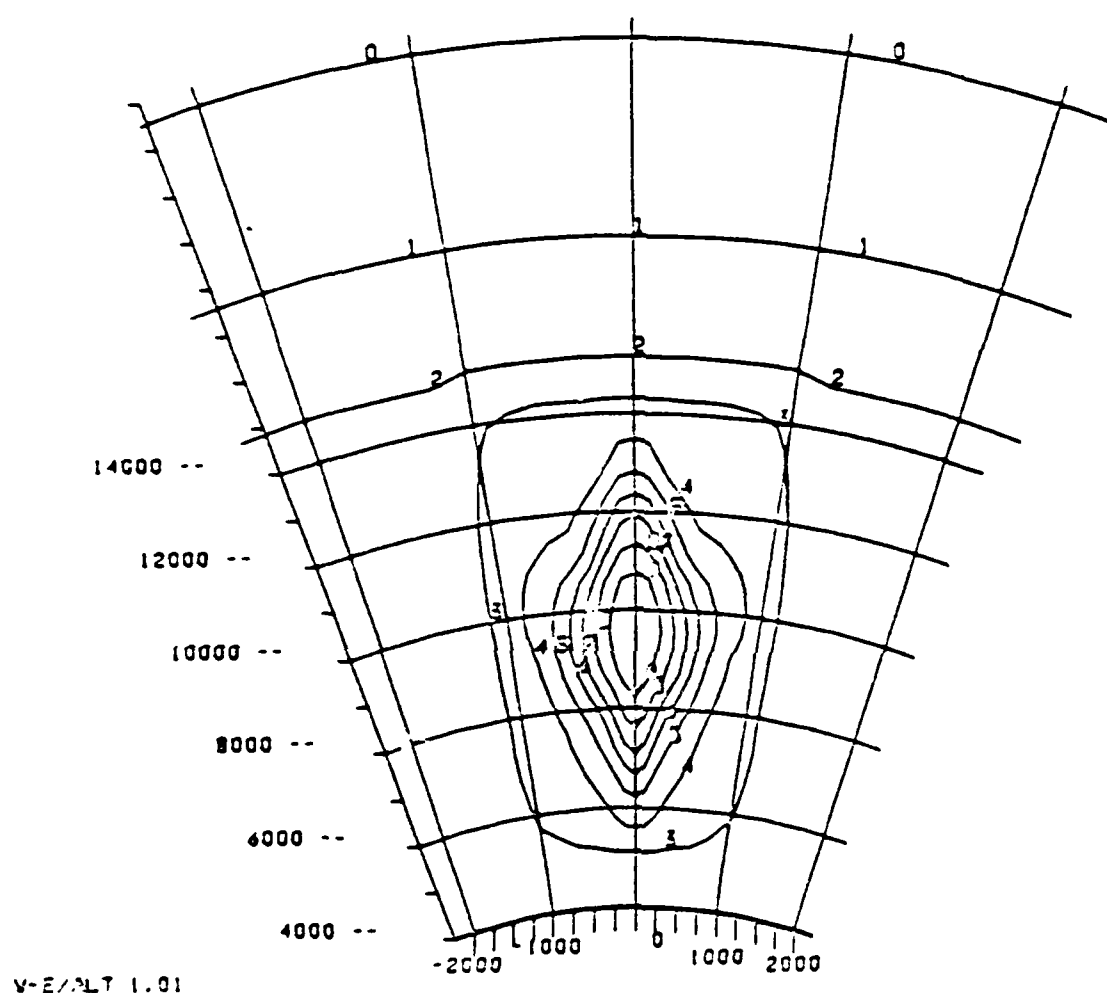
NLCY

Figure 7. A contour plot of the initial condition neutral atmospheric density at 300 seconds on the southern conjugate central meridian plane. Contour levels are shown in gauss  $\text{cm}^{-3}$  at the bottom of the graph.

INTEGRATED NE : X=0

TIME 3.00E 02

V-E ALT PLANE  
AT S-N 0



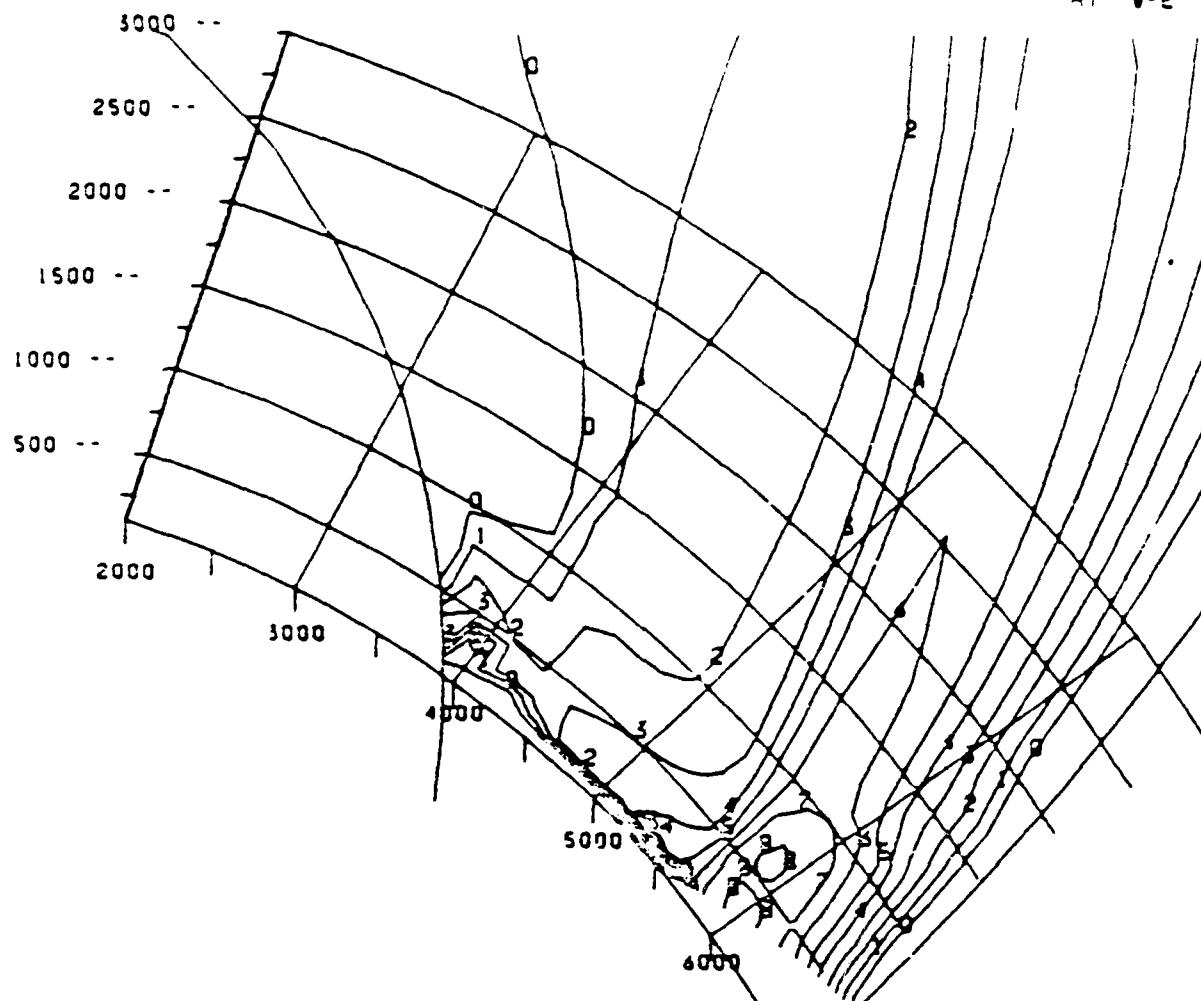
0. 1.0E 12    1. 3.0E 12    2. 1.0E 13    3. 3.0E 13    4. 1.0E 14

5. 3.0E 14    6. 1.0E 15    7. 3.0E 15    8. 1.0E 16    9. 3.0E 16    NLCY

Figure 8. A contour plot of the field line integrated electron density at 300 seconds on the geomagnetic equatorial plane. Contour levels, shown at the bottom of the plot, are in electrons  $\text{cm}^{-2}$ . The vertical scale is kilometer altitude and the horizontal scale is kilometers longitude at the earth's surface.

NE AT PHI = 0

TIME 1.80E 03

S-N ALT PLANE  
AT V-E 0

S-N/ALT 1.00

0 • 1.0E 04    1 • 3.0E 04    2 • 1.0E 05    3 • 3.0E 05    4 • 1.0E 06  
 5 • 3.0E 06    6 • 1.0E 07    7 • 3.0E 07    8 • 1.0E 08

NLCY

Figure 9. A contour plot of the electron density in the northern conjugate central meridian plane at 1800 seconds from the DEMAG simulation. Note the northward motion of the plasma plume relative to its location at 300 seconds in Figure 4. The plasma densities have also fallen by about a factor of 3 at the lower altitudes.

[illegible]

NLCY

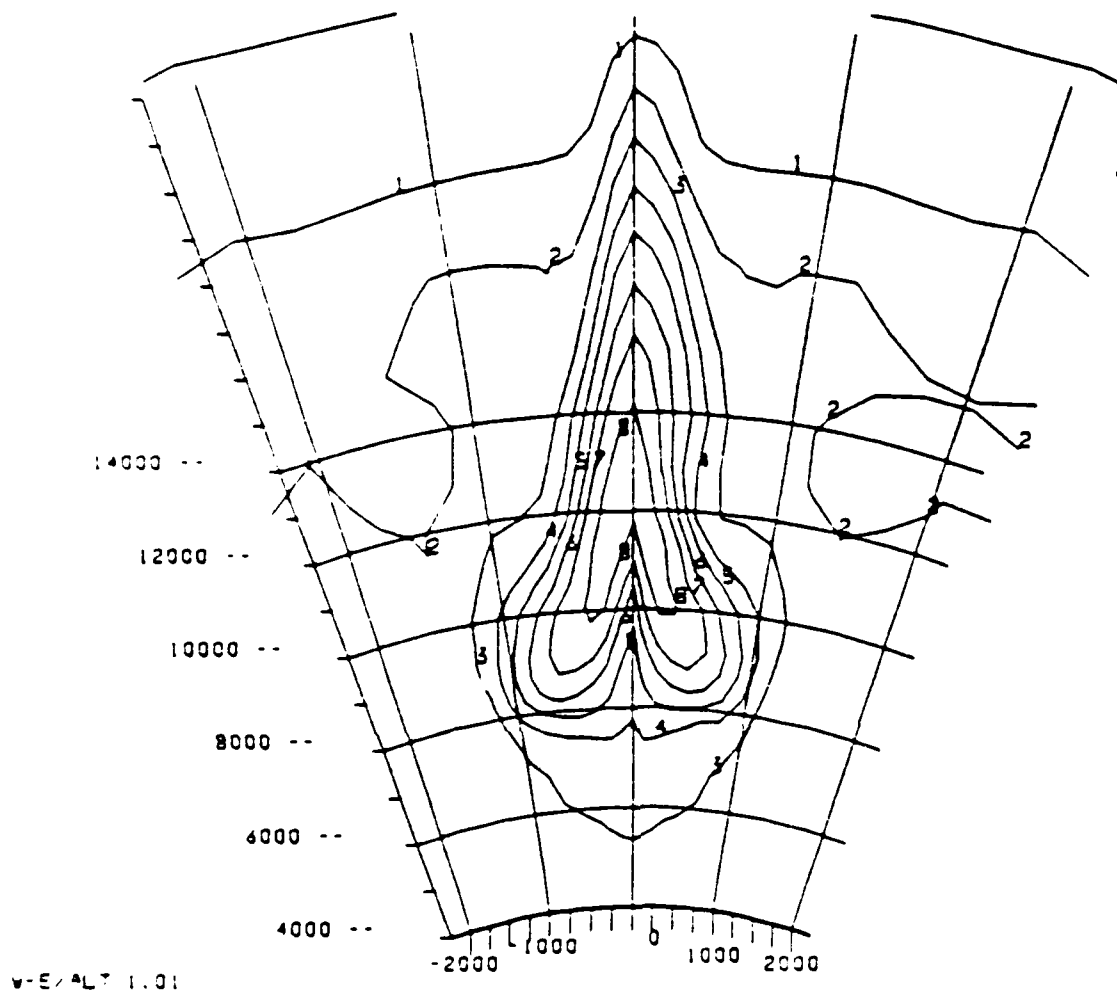
27



INTEGRATED NE  $\times 0$

TIME 1.80E 03

V-E ALT PLANE  
AT S-N 0

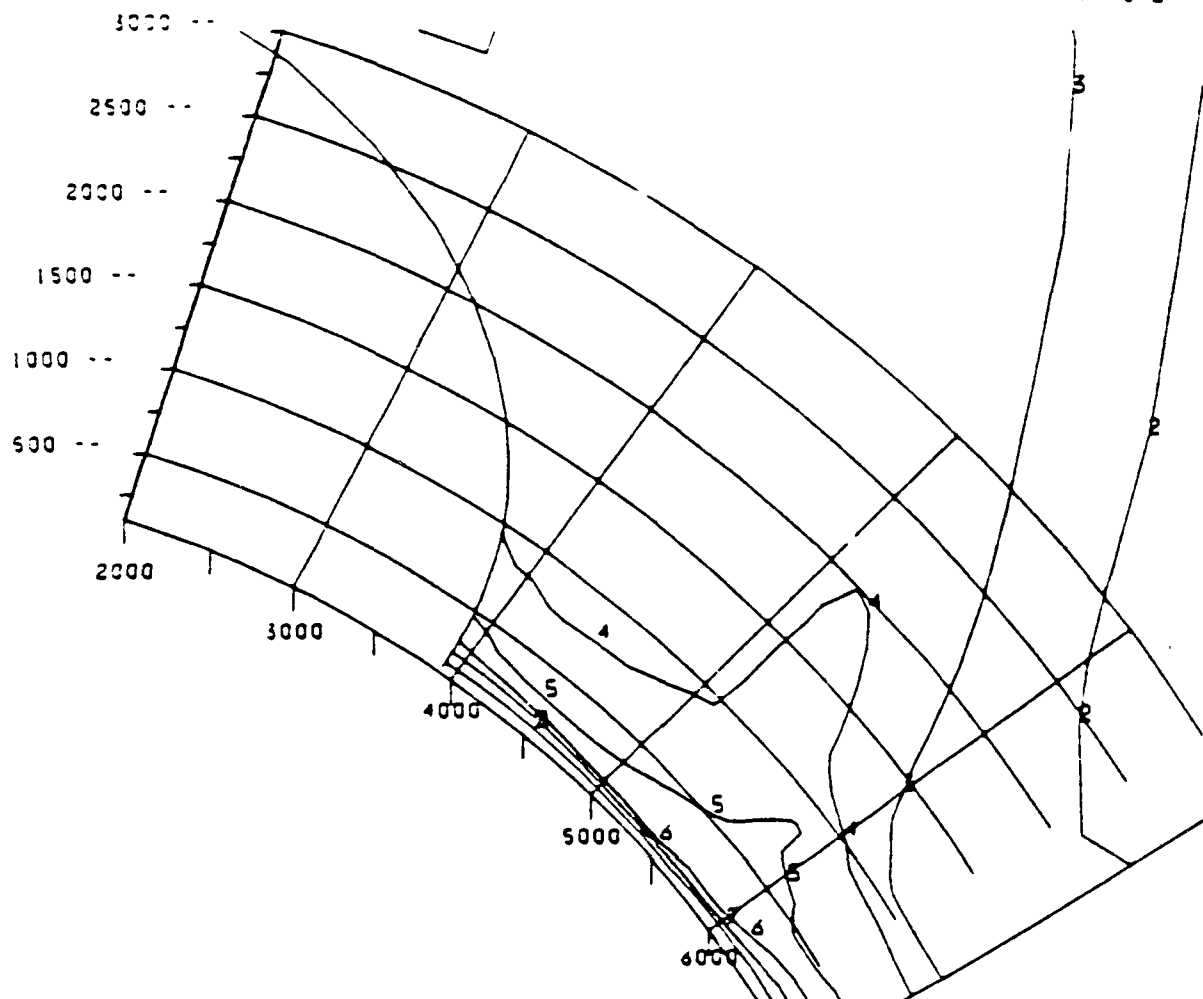


0. 1.0E 12    1. 3.0E 12    2. 1.0E 13    3. 3.0E 13    4. 1.0E 14  
5. 3.0E 14    6. 1.0E 15    7. 3.0E 15    8. 1.0E 16

NLCY

Figure 11. A contour plot of the field line integrated electron density in the geomagnetic equatorial plane at 1800 seconds from the DEMAG simulation. In comparing this plot to Figure 8 we note that the central portion of the plasma plume has moved dramatically upward and poleward. However, the eastward and westward portions of the plume have moved very little.

E-N ALT PLANE  
AT V-E 0



0 = 1.0E-20	1 = 1.0E-19	2 = 1.0E-18	3 = 1.0E-17	4 = 1.0E-16
5 = 1.0E-15	6 = 1.0E-14	7 = 1.0E-13	8 = 1.0E-12	

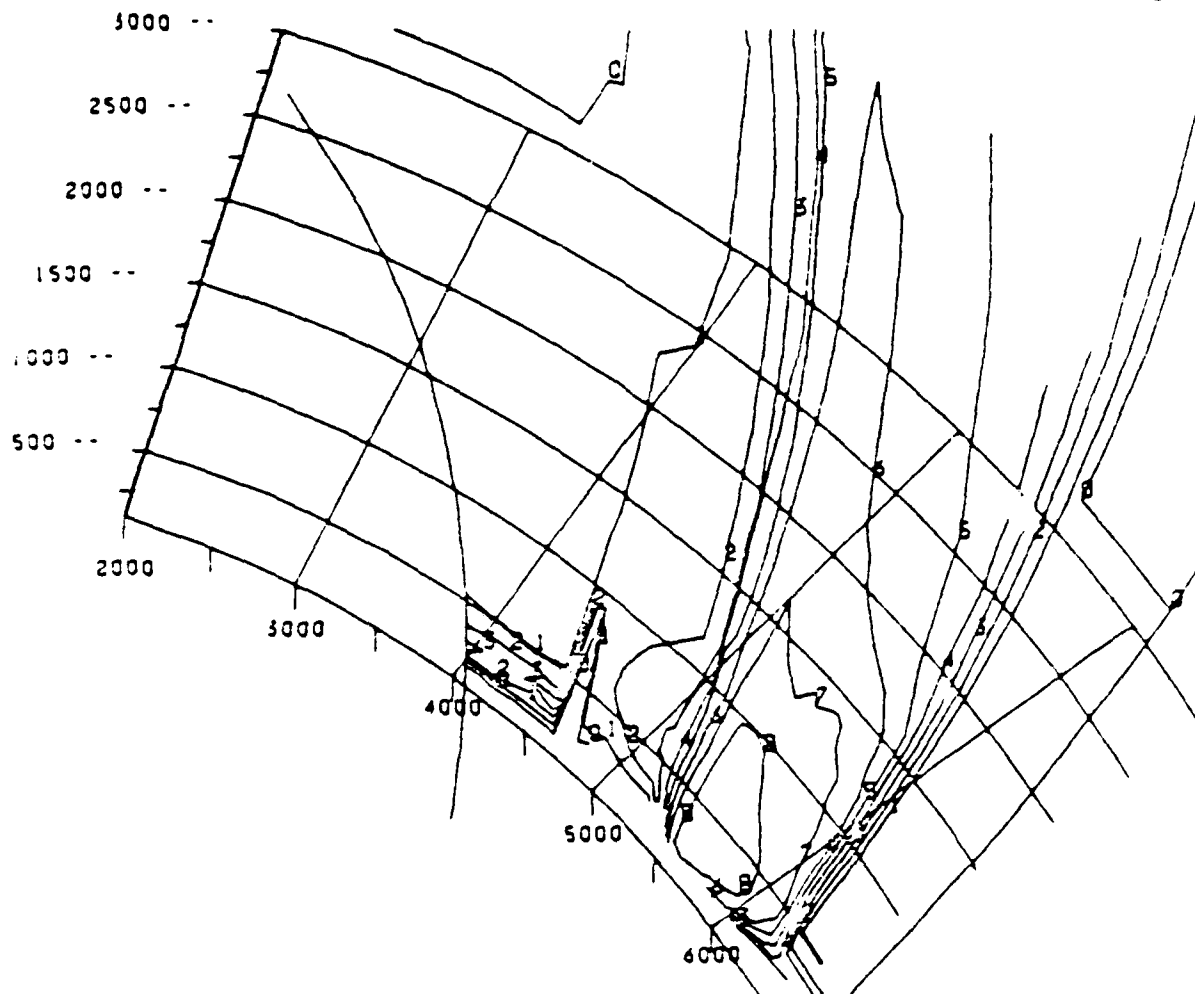
NLCY

Figure 12. A contour plot of the neutral atmospheric density in the northern conjugate central meridian plane at 1800 seconds from the DEMAG simulation. By this time the neutral atmospheric density has almost returned to its ambient values.

NE AT PHI = 0

TIME 1.80E 03

S-N ALT PLANE  
AT V-E 0



S-N/ALT 1.00

0 • 1.0E 04    1 • 3.0E 04    2 • 1.0E 05    3 • 3.0E 05    4 • 1.0E 06  
5 • 3.0E 06    6 • 1.0E 07    7 • 3.0E 07    8 • 1.0E 08

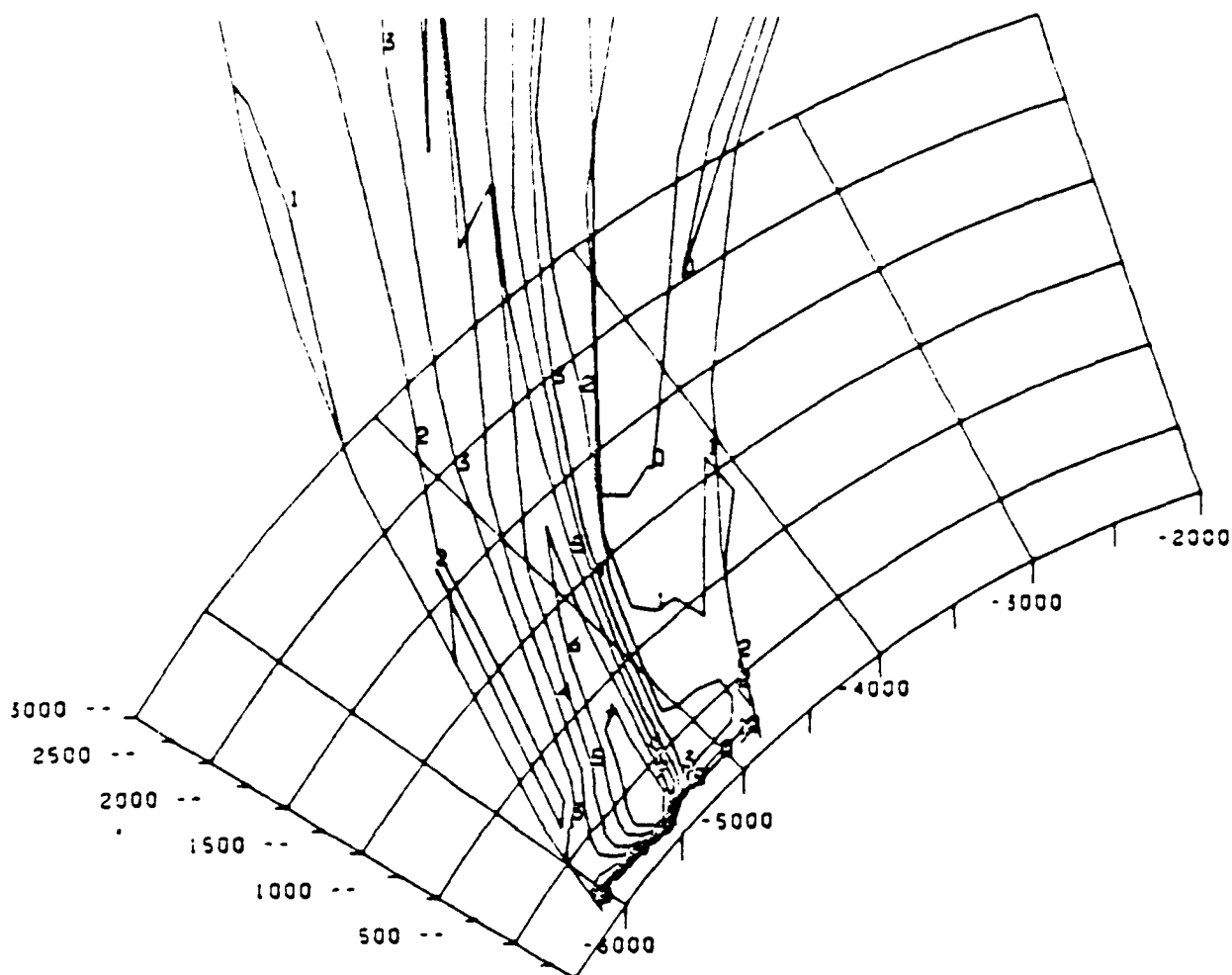
MCEY

Figure 13. A contour plot of the electron density from the MELT simulation in the northern conjugate central meridian plane at 1800 seconds. These results are to be compared to the DEMAG results in Figure 9.

NE AT 04:00

TIME 1.80E 03

S-N ALT PLANE  
AT V-E 0



S-N/ALT 1.00

0 • 1.0E 04	1 • 3.0E 04	2 • 1.0E 05	3 • 3.0E 05	4 • 1.0E 06
5 • 3.0E 06	6 • 1.0E 07	7 • 3.0E 07		

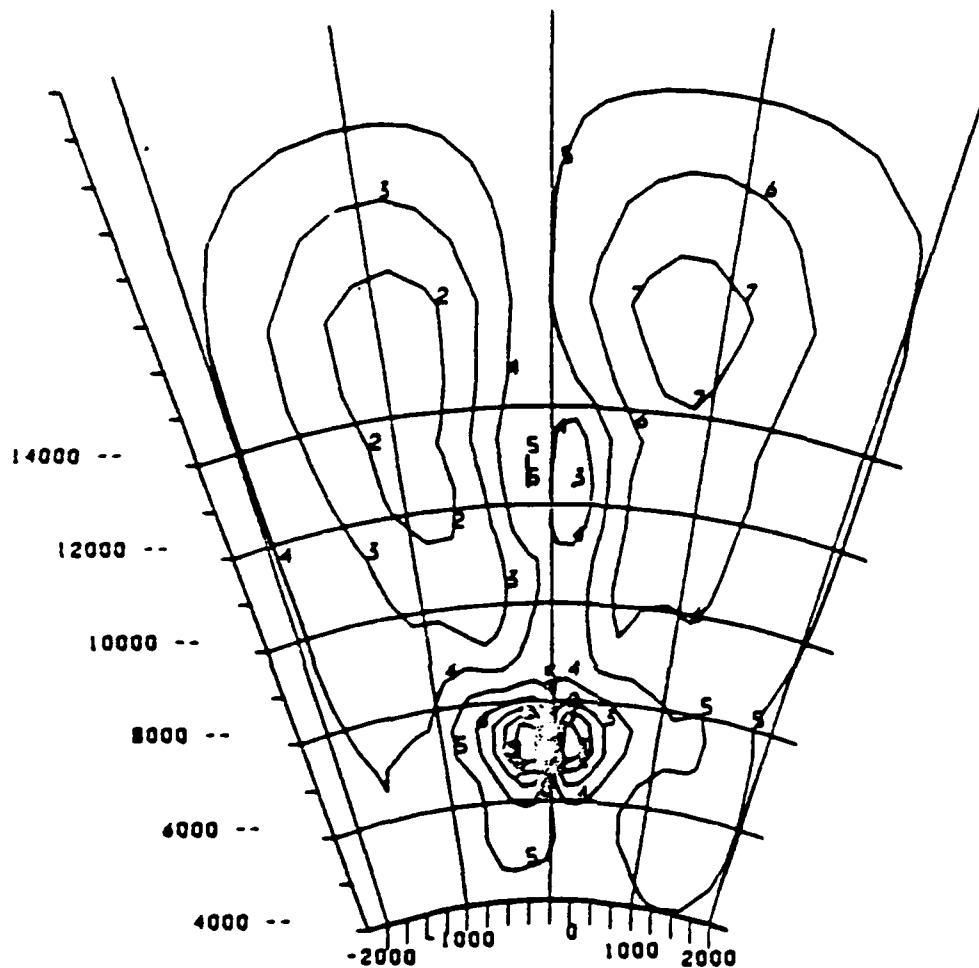
MCEY

Figure 14. A contour plot of the electron density from the MELT simulation in the southern conjugate central meridian plane at 1800 seconds. These results are to be compared to the DEMAG results in Figure 10.

PSI (STAT. VOLTS)

TIME 6.03E 02

V-E ALT PLANE  
AT S-N 0



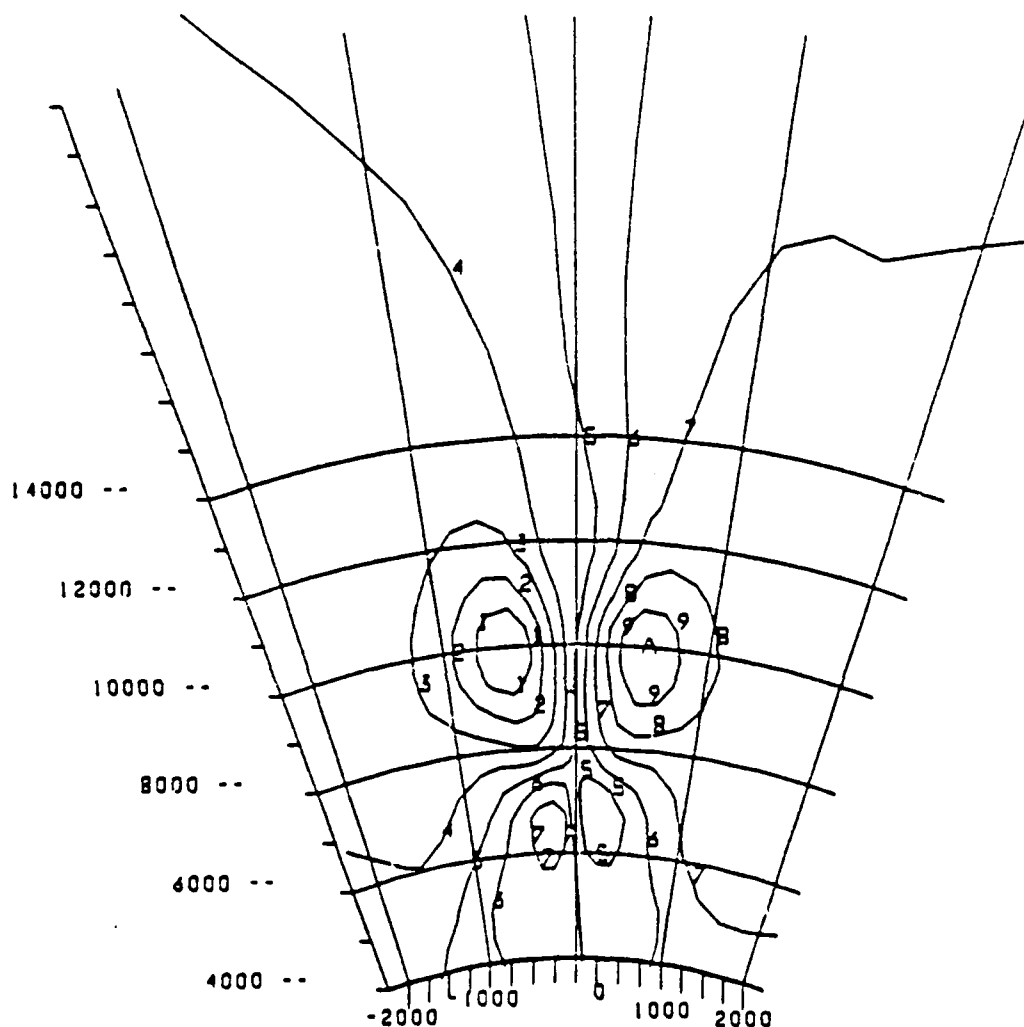
1--3.0E 00    2--5.9E 00    3--3.7E 00    4--1.5E 00    5- 6.2E-01  
6- 2.1E 00    7- 4.9E 00    8- 7.1E 00    9- 9.3E 00    A- 1.1E 01    NLCY

Figure 15. A contour plot of the electrostatic potential at 600 seconds for the DEMAG simulation shown on the geomagnetic equatorial plane. The contour levels are shown at the bottom of the diagram for the potential and are in stat volts. See text for a discussion of the results.

PSI (STAT. VOLTS)

TIME 6.00E 02

V-E ALT FL  
AT S-N



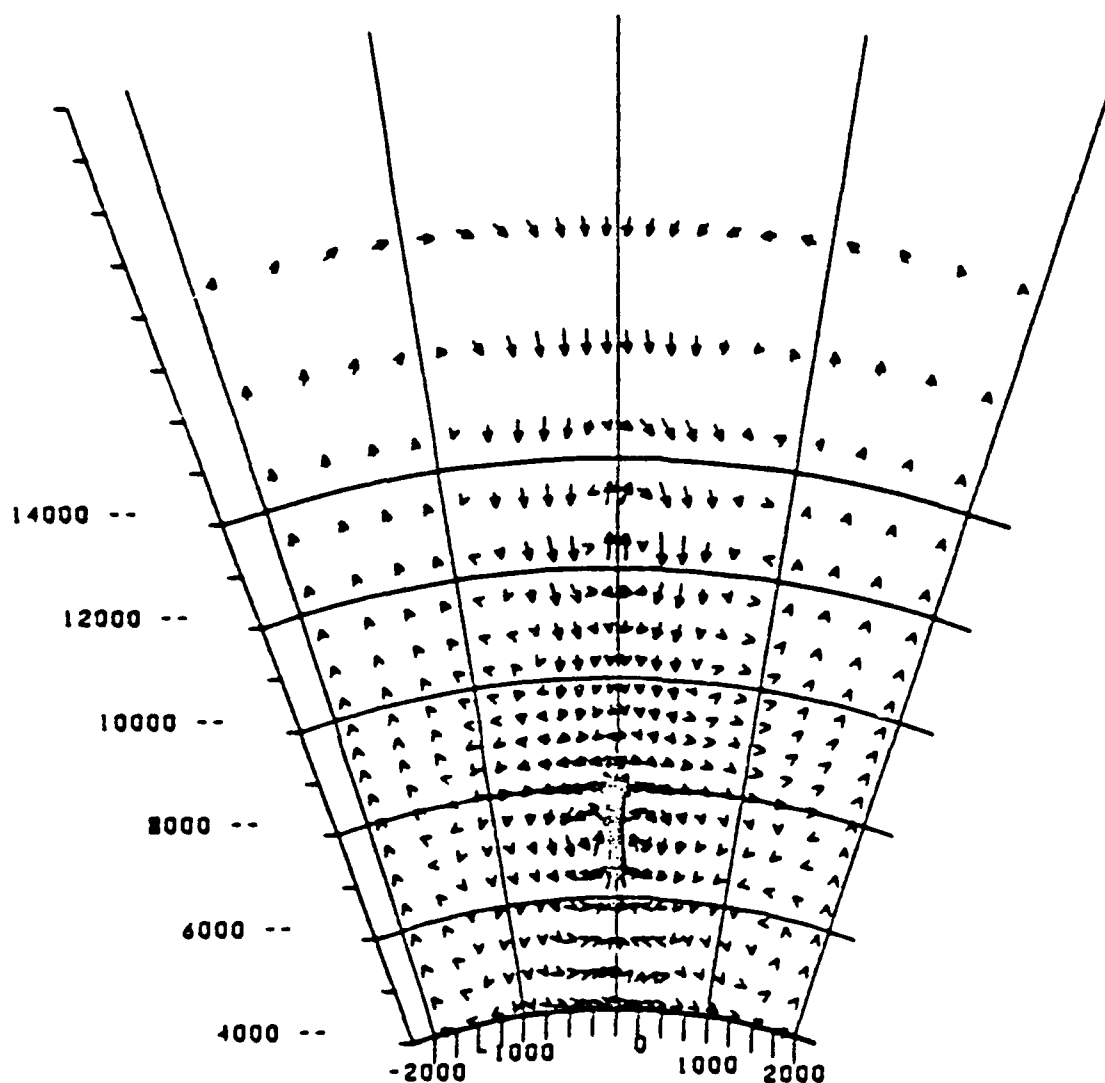
1--2.0E 01 2--1.5E 01 3--1.1E 01 4--6.7E 00 5--2.3E 00  
6--2.1E 00 7--6.5E 00 8--1.1E 01 9--1.5E 01 A--2.0E 01 MCE

Figure 16. A contour plot of the electrostatic potential at 600 seconds for the MELT simulation shown on the geomagnetic equatorial plane. The contour levels are shown at the bottom of the diagram for the potential in stat volts.

PLASMA VELOCITY

TIME 6.03E 02

V-I ALT PLANE  
AT 3-4 0



V-E -COMP.1MAX.1 1.0024E 05 ALT -COMP.1MAX.1 2.9787E 05

UNIT LENGTH 2.9787E 05

NLCY

Figure 17. A vector plot of the velocity perpendicular to the geomagnetic field in the equatorial plane for the DEMAG simulations at 600 seconds. The velocity scale is shown at the bottom in  $\text{cm sec}^{-1}$ . See text for a discussion.

PLASMA VELOCITY

TIME 6.00E 02

V-E - COMP. 1  
ALT - COMP. 1

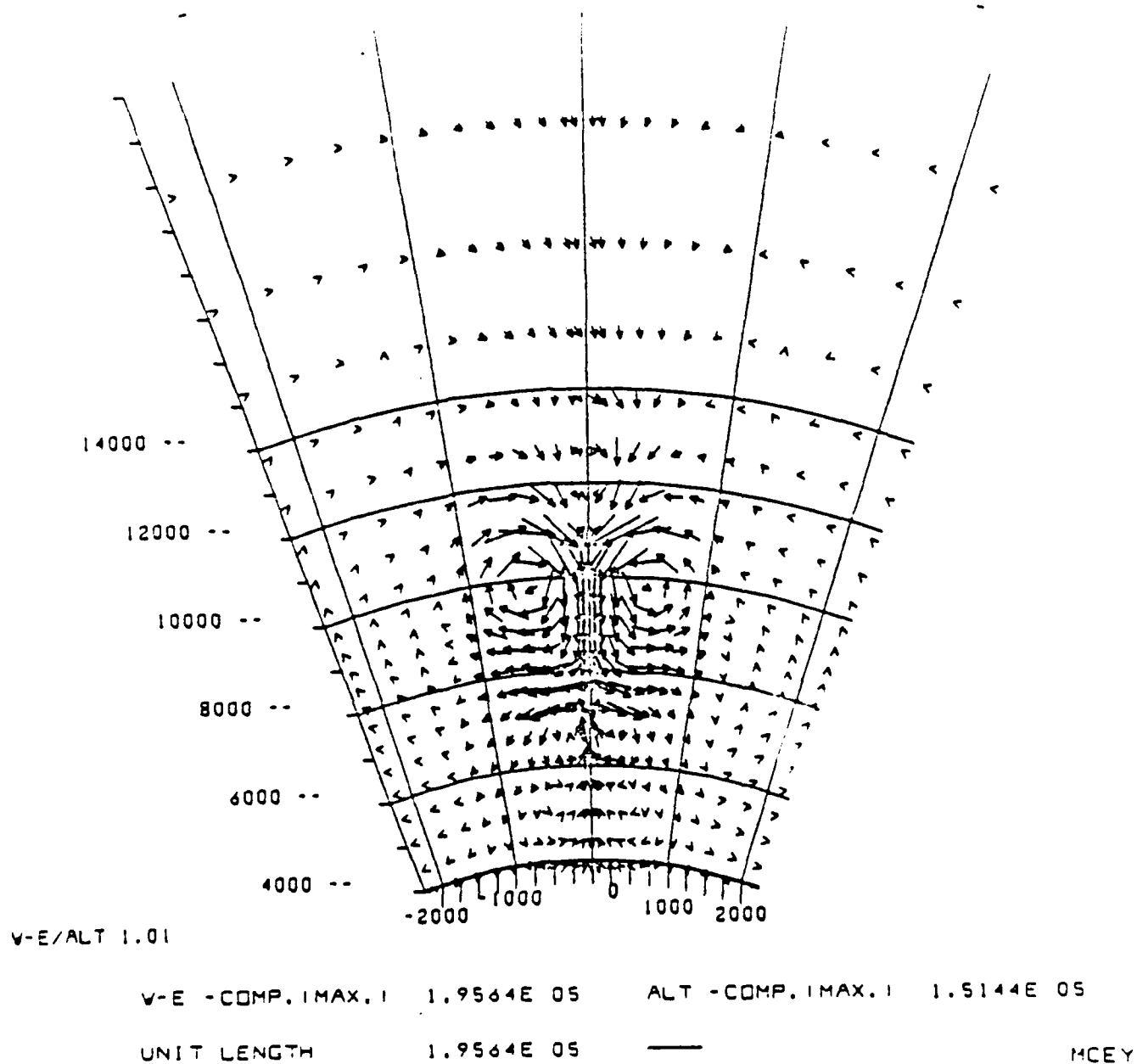
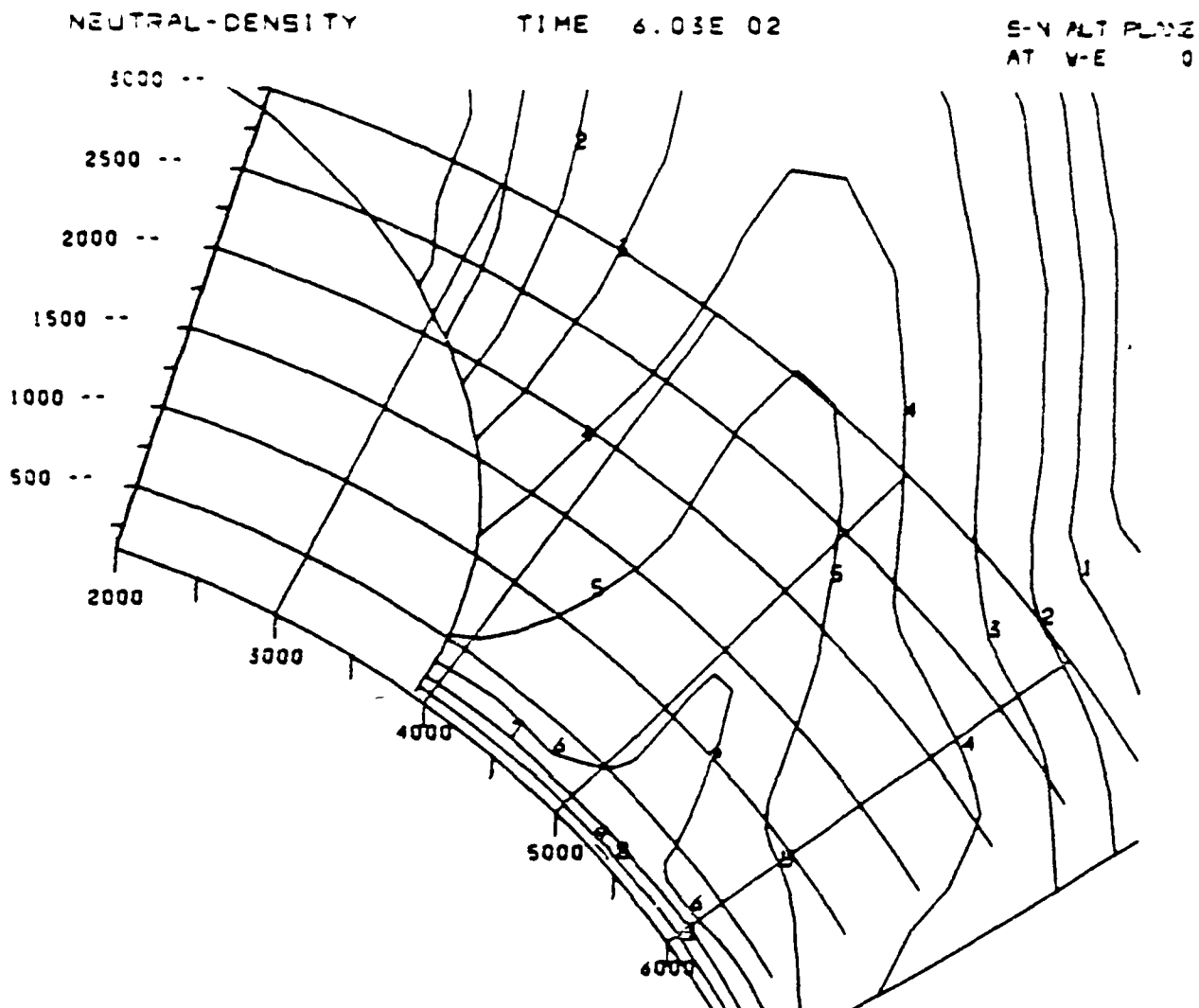


Figure 18. A vector plot of the velocity perpendicular to the geomagnetic field in the equatorial plane for the MELT simulation at 600 seconds. The velocity scale is shown in  $\text{cm sec}^{-1}$ .





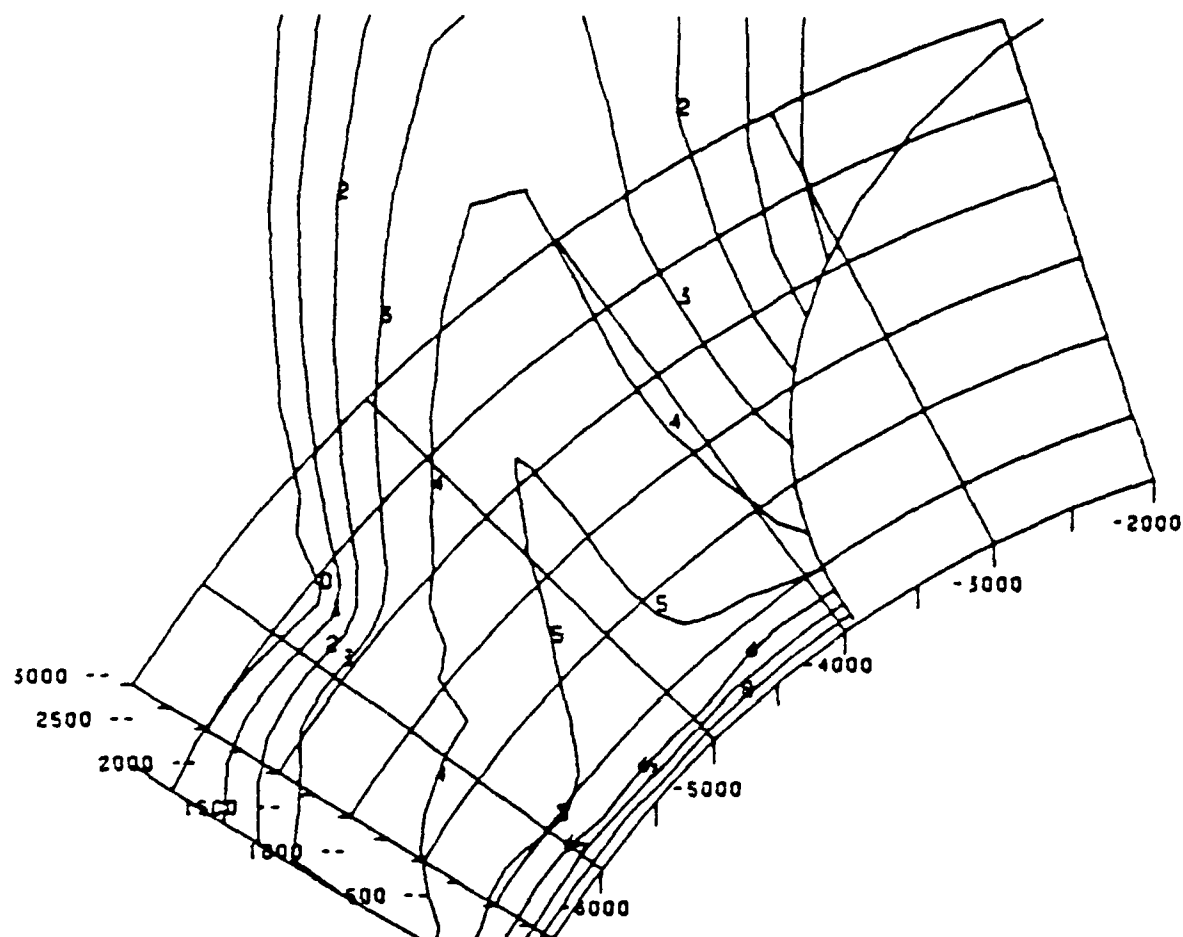
0 •  $1.0E-20$     1 •  $1.0E-19$     2 •  $1.0E-18$     3 •  $1.0E-17$     4 •  $1.0E-16$   
 5 •  $1.0E-15$     6 •  $1.0E-14$     7 •  $1.0E-13$     8 •  $1.0E-12$     9 •  $1.0E-11$     NLCY

Figure 19. A contour plot of the neutral atmospheric density in the northern conjugate central meridian plane for the DEMAG simulation at 600 secs. Notice the high densities above 1500 km altitude which are not considered in the MELT simulation.

NEUTRAL-DENSITY

TIME 6.03E 02

S-N ALT PLANE  
AT V-E 0



0 • 1.0E-20    1 • 1.0E-19    2 • 1.0E-18    3 • 1.0E-17    4 • 1.0E-16

5 • 1.0E-15    6 • 1.0E-14    7 • 1.0E-13    8 • 1.0E-12

NLCY

Figure 20. A contour plot of the neutral atmospheric density in the southern conjugate central meridian plane for the DEMAG simulation at 600 secs. Similar comments to those for Figure 19 apply.

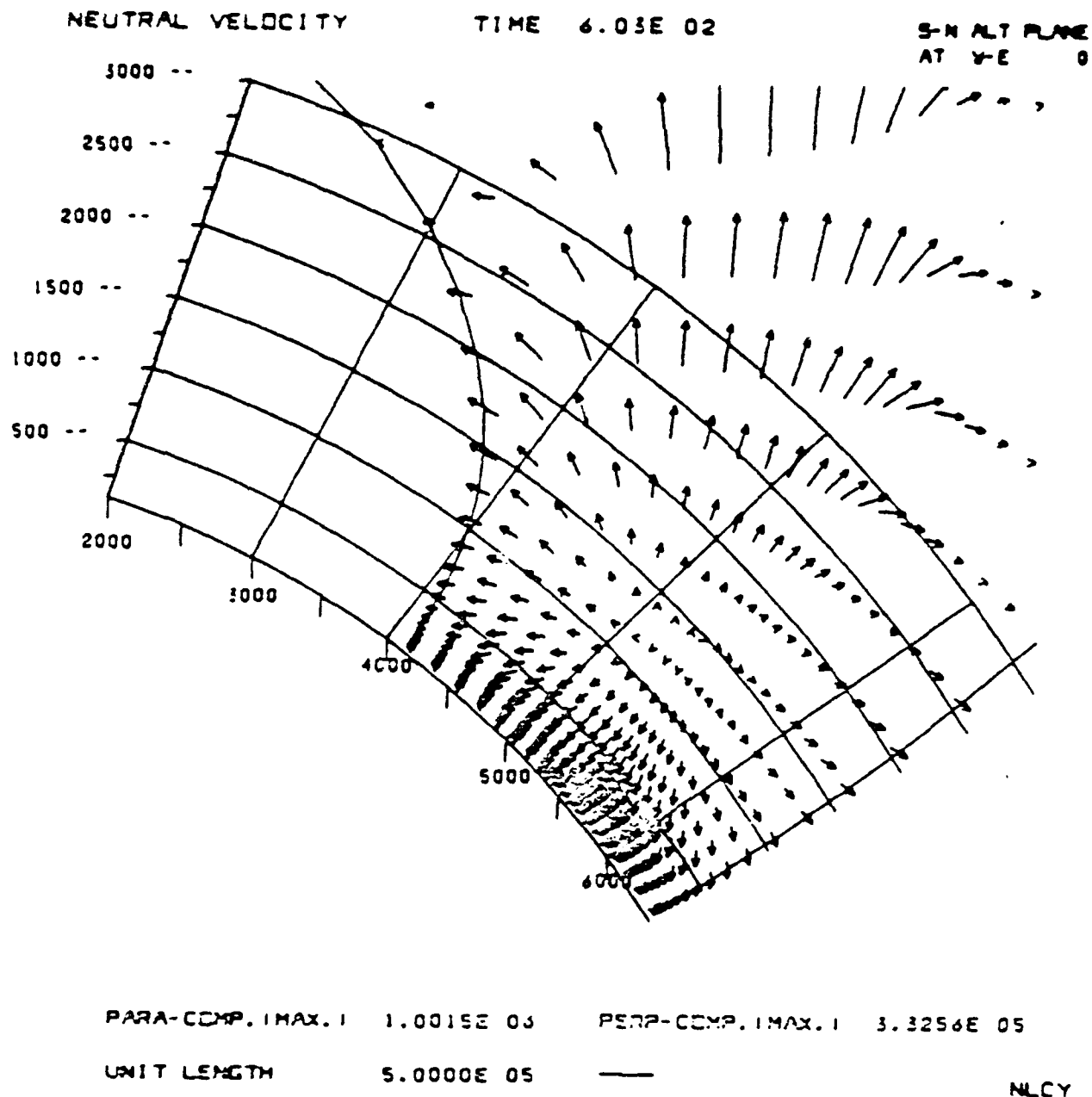
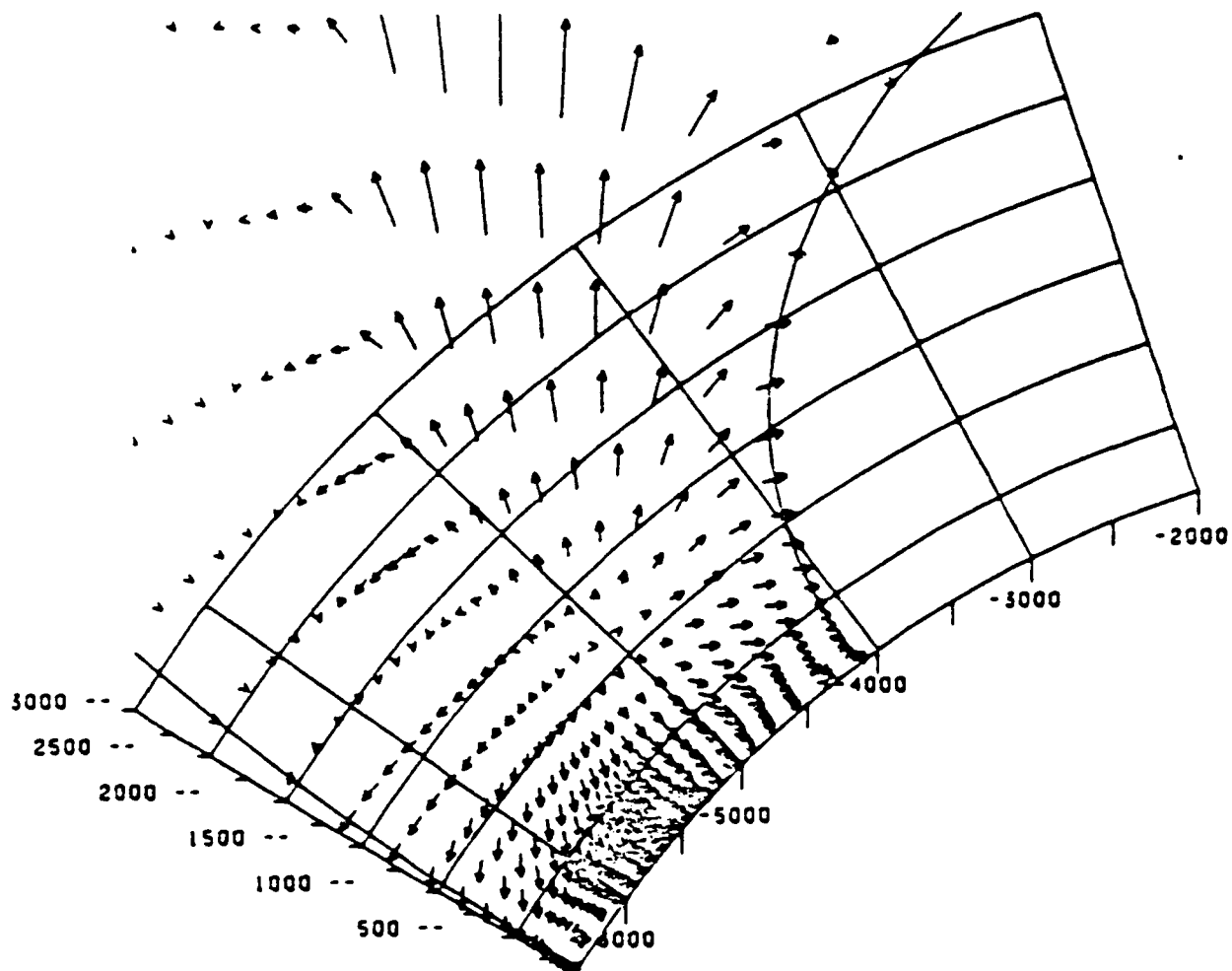


Figure 21. A vector plot of neutral velocity for the DEMAG simulation in the northern conjugate central meridian plane at 600 seconds. Notice the large upward and poleward, relative to the geomagnetic field, velocities at altitudes above 1500 kilometers.

NEUTRAL-VELOCITY

TIME 6.03E 02

S-N ALT PLANE  
AT Y-E 0

PARA-COMP.1MAX.1 9.6343E 05 PERP-COMP.1MAX.1 3.5136E 05

UNIT LENGTH 5.0000E 05

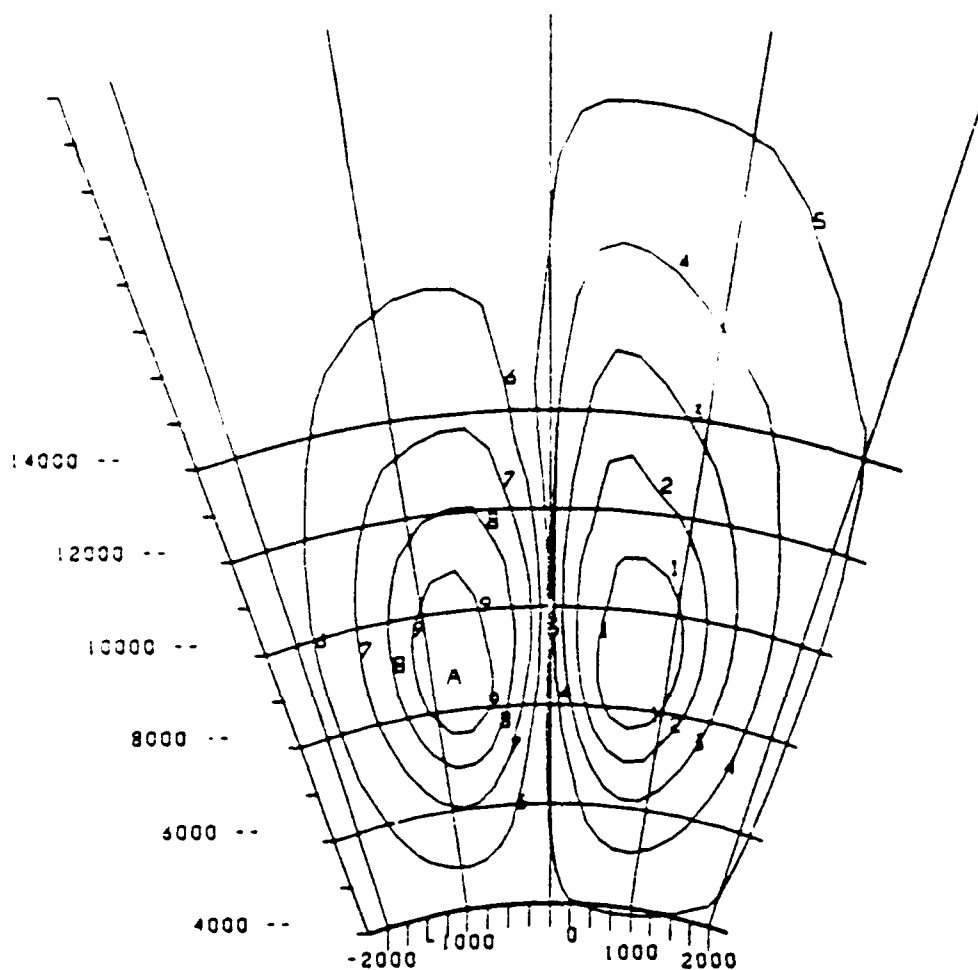
NLCY

Figure 22. A vector plot of neutral velocity for the DEMAG simulation in the southern conjugate central meridian plane at 600 seconds. Comments similar to those for Figure 21 apply.

PS: (STAT. VOLTS)

TIME 1.80E 03

V-E ALT PLANE  
AT S-N 0



1\*-1.6E 01 2\*-1.2E 01 3\*-8.4E 00 4\*-4.6E 00 5\*-8.0E-01

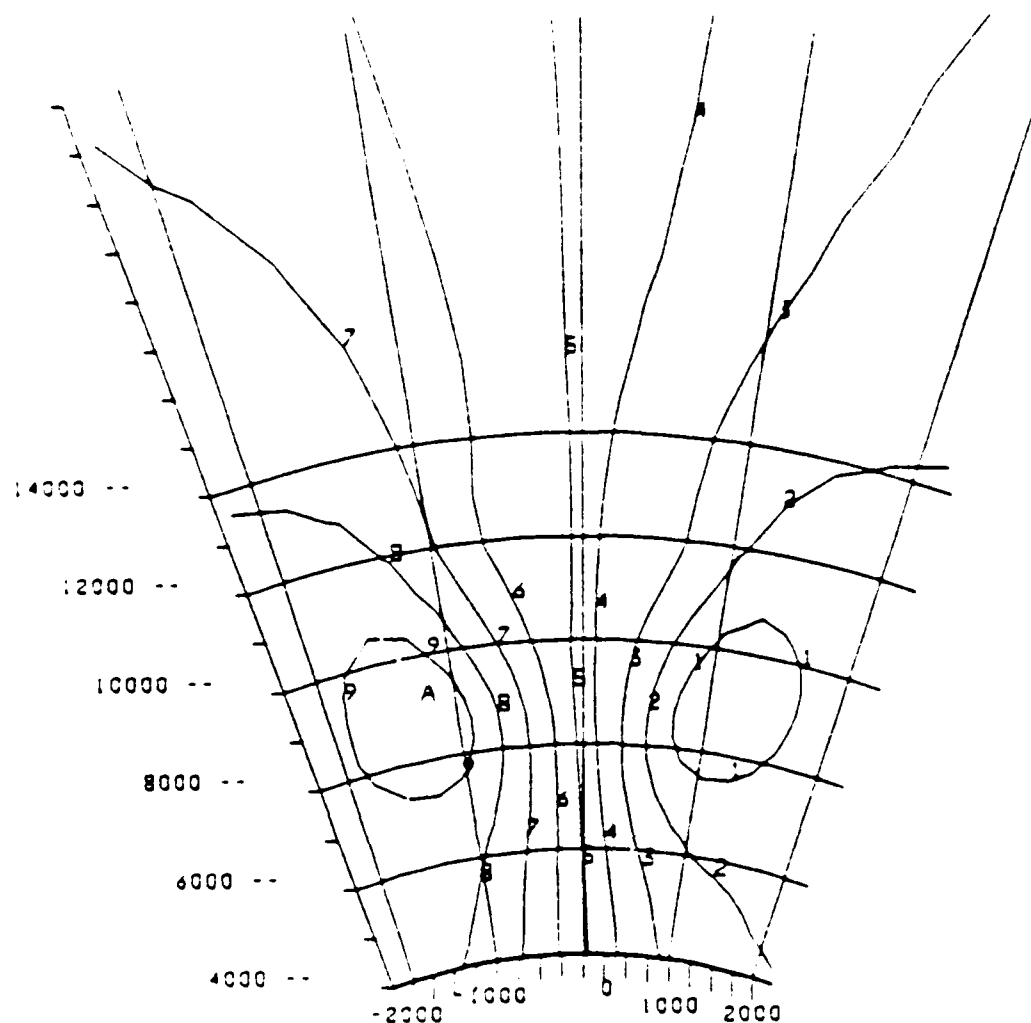
6\* 3.0E 00 7\* 6.8E 00 8\* 1.1E 01 9\* 1.4E 01 A\* 1.9E 01 NLCY

Figure 23. A contour plot of the electrostatic potential for the DEMAG simulation in the geomagnetic equatorial plane at 1800 seconds. Refer to the text for discussion.

PS: (STAT. VOLTS)

TIME 1.80E 03

V-E ALT PLANE  
AT S-N 0



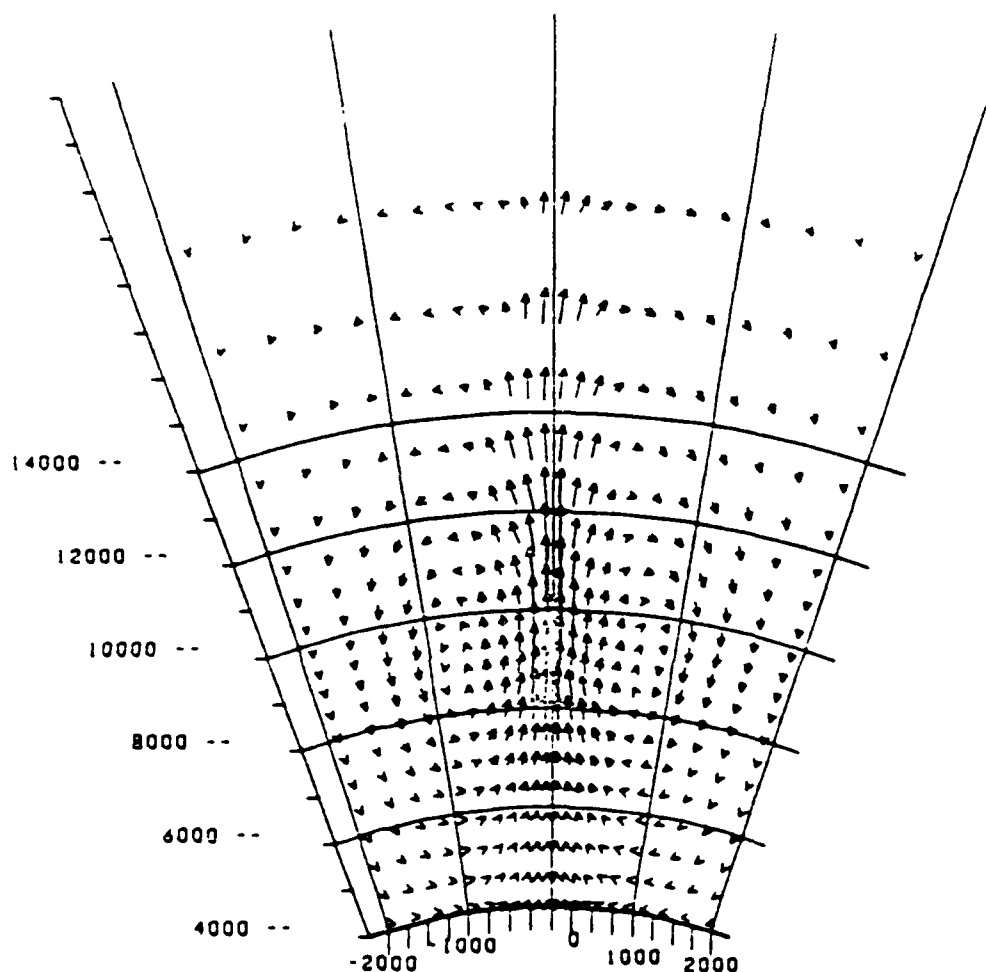
1:-4.8E 01 2:-3.6E 01 3:-2.3E 01 4:-1.1E 01 5: 1.1E 00  
6: 1.3E 01 7: 2.4E 01 8: 3.8E 01 9: 5.0E 01 A: 6.0E 01 MCEV

Figure 24. A contour plot of the electrostatic potential for the MELT simulation in the geomagnetic equatorial plane at 1800 seconds.

PLASMA VELOCITY

TIME 1.80E 03

V-E ALT PLANE  
AT S-N 0

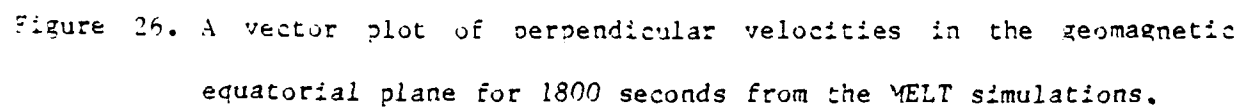


V-E -COMP.1MAX.1 7.0697E 04 ALT -COMP.1MAX.1 3.7830E 05

UNIT LENGTH 3.7830E 05 ——— NLCY

Figure 25. A vector plot of perpendicular velocities in the geomagnetic equatorial plane for 1800 seconds from the DEMAG simulation. Refer to the text for discussion.

V-E ALT PLANE  
AT S-N 0





## References

- Hain, K. and J. Fedder, "Electrostatic equations for large scale plasma simulation studies," NRL Memo Rept. 5385, 1984.
- Kilb, R.W., "Striation Formation," in Physics of High Altitude Nuclear Burst Effects, DNA 4501F, 1977.
- Longmire, C.L. and R.W. Kilb, "Plasma Physics," in Physics of High Altitude Nuclear Burst Effects, DNA 4501F, 1977.

DISTRIBUTION LIST

DEPARTMENT OF DEFENSE

ASSISTANT SECRETARY OF DEFENSE  
COMM, CMD, CONT 7 INTELL  
WASHINGTON, D.C. 20301

DIRECTOR  
COMMAND CONTROL TECHNICAL CENTER  
PENTAGON RM BE 685  
WASHINGTON, D.C. 20301  
01CY ATTN C-650  
01CY ATTN C-312 R. MASON

DIRECTOR  
DEFENSE ADVANCED RSCH PROJ AGENCY  
ARCHITECT BUILDING  
1400 WILSON BLVD.  
ARLINGTON, VA. 22209  
01CY ATTN NUCLEAR  
MONITORING RESEARCH  
01CY ATTN STRATEGIC TECH OFFICE

DEFENSE COMMUNICATION ENGINEER CENTER  
1860 WIEHLE AVENUE  
RESTON, VA. 22090  
01CY ATTN CODE R410  
01CY ATTN CODE R812

DEFENSE TECHNICAL INFORMATION CENTER  
CAMERON STATION  
ALEXANDRIA, VA. 22314  
02CY

DIRECTOR  
DEFENSE NUCLEAR AGENCY  
WASHINGTON, D.C. 20305  
01CY ATTN STVL  
04CY ATTN TITL  
01CY ATTN DDST  
03CY ATTN RAEE

COMMANDER  
FIELD COMMAND  
DEFENSE NUCLEAR AGENCY  
KIRTLAND, AFB, NM 87115  
01CY ATTN FCPR

DEFENSE NUCLEAR AGENCY  
SAO/DNA  
BUILDING 20676  
KIRTLAND AFB, NM 87115  
01CY D.C. THORNBURG

DIRECTOR  
INTERSERVICE NUCLEAR WEAPONS SCHOOL  
KIRTLAND AFB, NM 87115  
01CY ATTN DOCUMENT CONTROL

JOINT CHIEFS OF STAFF  
WASHINGTON, D.C. 20301  
01CY ATTN J-3 WWMCCS EVALUATION  
OFFICE

DIRECTOR  
JOINT STRAT TGT PLANNING STAFF  
OFFUTT AFB  
OMAHA, NB 68113  
01CY ATTN JSTPS/JLKS  
01CY ATTN JPST G. GOETZ

CHIEF  
LIVERMORE DIVISION FLD COMMAND DNA  
DEPARTMENT OF DEFENSE  
LAWRENCE LIVERMORE LABORATORY  
P.O. BOX 808  
LIVERMORE, CA 94550  
01CY ATTN FCPRL

COMMANDANT  
NATO SCHOOL (SHAPE)  
APO NEW YORK 09172  
01CY ATTN U.S. DOCUMENTS OFFICER

UNDER SECY OF DEF FOR RSCH & ENGRG  
DEPARTMENT OF DEFENSE  
WASHINGTON, D.C. 20301  
01CY ATTN STRATEGIC & SPACE  
SYSTEMS (OS)

WWMCCS SYSTEM ENGINEERING ORG  
WASHINGTON, D.C. 20305  
01CY ATTN R. CRAWFORD

COMMANDER/DIRECTOR  
ATMOSPHERIC SCIENCES LABORATORY  
U.S. ARMY ELECTRONICS COMMAND  
WHITE SANDS MISSILE RANGE, NM 88002  
O1CY ATTN DELAS-EO, F. NILES

DIRECTOR  
BMD ADVANCED TECH CTR  
HUNTSVILLE OFFICE  
P.O. BOX 1500  
HUNTSVILLE, AL 35807  
O1CY ATTN ATC-T MELVIN T. CAPPS  
O1CY ATTN ATC-O W. DAVIES  
O1CY ATTN ATC-R DON RUSS

PROGRAM MANAGER  
BMD PROGRAM OFFICE  
5001 EISENHOWER AVENUE  
ALEXANDRIA, VA 22333  
O1CY ATTN DACS-BMT J. SHEA

CHIEF C-E- SERVICES DIVISION  
U.S. ARMY COMMUNICATIONS CMD  
PENTAGON RM 1B269  
WASHINGTON, D.C. 20310  
O1CY ATTN C- E-SERVICES DIVISION

COMMANDER  
FRADCOM TECHNICAL SUPPORT ACTIVITY  
DEPARTMENT OF THE ARMY  
FORT MONMOUTH, N.J. 07703  
O1CY ATTN DRSEL-NL-RD H. BENNET  
O1CY ATTN DRSEL-PL-ENV H. BOMKE  
O1CY ATTN J.E. QUIGLEY

COMMANDER  
U.S. ARMY COMM-ELEC ENGRG INSTAL AGY  
FT. HUACHUCA, AZ 85613  
O1CY ATTN CCC-EMEO GEORGE LANE

COMMANDER  
U.S. ARMY FOREIGN SCIENCE & TECH CTR  
220 7TH STREET, NE  
CHARLOTTESVILLE, VA 22901  
O1CY ATTN DRXST-SD

COMMANDER  
U.S. ARMY MATERIAL DEV & READINESS CMD  
5001 EISENHOWER AVENUE  
ALEXANDRIA, VA 22333  
O1CY ATTN DRCLDC J.A. BENDER

COMMANDER  
U.S. ARMY NUCLEAR AND CHEMICAL AGENCY  
7500 BACKLICK ROAD  
BLDG 2073  
SPRINGFIELD, VA 22150  
O1CY ATTN LIBRARY

DIRECTOR  
U.S. ARMY BALLISTIC RESEARCH-  
LABORATORY  
ABERDEEN PROVING GROUND, MD 21005  
O1CY ATTN TECH LIBRARY,  
EDWARD BAICY

COMMANDER  
U.S. ARMY SATCOM AGENCY  
FT. MONMOUTH, NJ 07703  
O1CY ATTN DOCUMENT CONTROL

COMMANDER  
U.S. ARMY MISSILE INTELLIGENCE AGENCY  
REDSTONE ARSENAL, AL 35809  
O1CY ATTN JIM GAMBLE

DIRECTOR  
U.S. ARMY TRADOC SYSTEMS ANALYSIS  
ACTIVITY  
WHITE SANDS MISSILE RANGE, NM 88002  
O1CY ATTN ATAA-SA  
O1CY ATTN TCC/F. PAYAN JR.  
O1CY ATTN ATTA-TAC LTC J. HESSE

COMMANDER  
NAVAL ELECTRONIC SYSTEMS COMMAND  
WASHINGTON, D.C. 20360  
O1CY ATTN NAVALEX 034 T. HUGHES  
O1CY ATTN PME 117  
O1CY ATTN PME 117-T  
O1CY ATTN CODE 5011

COMMANDING OFFICER  
NAVAL INTELLIGENCE SUPPORT CTR  
4301 SUITLAND ROAD, BLDG. 5  
WASHINGTON, D.C. 20390  
O1CY ATTN MR. DURBIN STIC 12  
O1CY ATTN NISC-50  
O1CY ATTN CODE 5404 J. GALET

COMMANDER  
NAVAL OCEAN SYSTEMS CENTER  
SAN DIEGO, CA 92152  
O1CY ATTN J. FERGUSON

NAVAL RESEARCH LABORATORY

WASHINGTON, D.C. 20375

01CY ATTN CODE 4700 S. L. Ossakow  
26 CYS IF UNCLASS. 1 CY  
IF CLASS)

01CY ATTN CODE 4701 I Vitkovitsky

01CY ATTN CODE 4780 J. Huba (50  
CYS IF UNCLASS, 1 CY IF CLASS)

01CY ATTN CODE 7500

01CY ATTN CODE 7550

01CY ATTN CODE 7580

01CY ATTN CODE 7551

01CY ATTN CODE 7555

01CY ATTN CODE 4730 E. MCLEAN

01CY ATTN CODE 4108

01CY ATTN CODE 4730 B. RIPIN

20CY ATTN CODE 2628

COMMANDER

NAVAL SPACE SURVEILLANCE SYSTEM

DAHLGREN, VA 22448

01CY ATTN CAPT J.H. BURTON

OFFICER-IN-CHARGE

NAVAL SURFACE WEAPONS CENTER

WHITE OAK, SILVER SPRING, MD 20910

01CY ATTN CODE F31

DIRECTOR

STRATEGIC SYSTEMS PROJECT OFFICE

DEPARTMENT OF THE NAVY

WASHINGTON, D.C. 20376

01CY ATTN NSP-2141

01CY ATTN NSSP-2722 FRED WIMBERLY

COMMANDER

NAVAL SURFACE WEAPONS CENTER

DAHLGREN LABORATORY

DAHLGREN, VA 22448

01CY ATTN CODE DF-14 R. BUTLER

OFFICER OF NAVAL RESEARCH

ARLINGTON, VA 22217

01CY ATTN CODE 465

01CY ATTN CODE 461

01CY ATTN CODE 402

01CY ATTN CODE 420

01CY ATTN CODE 421

COMMANDER

AEROSPACE DEFENSE COMMAND/DC

DEPARTMENT OF THE AIR FORCE

ENT AFB, CO 80912

01CY ATTN DC MR. LONG

COMMANDER

AEROSPACE DEFENSE COMMAND/XPD

DEPARTMENT OF THE AIR FORCE

ENT AFB, CO 80912

01CY ATTN XPDQG

01CY ATTN XP

AIR FORCE GEOPHYSICS LABORATORY

HANSCOM AFB, MA 01731

01CY ATTN OPR HAROLD GARDNER

01CY ATTN LKB

KENNETH S.W. CHAMPION

01CY ATTN OPR ALVA T. STAIR

01CY ATTN PHD JURGEN BUCHAU

01CY ATTN PHD JOHN P. MULLEN

AF WEAPONS LABORATORY

KIRTLAND AFB, NM 87117

01CY ATTN SUL

01CY ATTN CA ARTHUR H. GUENTHER

01CY ATTN NTYCE 1LT. G. KRAJEI

AFTAC

PATRICK AFB, FL 32925

01CY ATTN TN

AIR FORCE AVIONICS LABORATORY

WRIGHT-PATTERSON AFB, OH 45433

01CY ATTN AAD WADE HUNT

01CY ATTN AAD ALLEN JOHNSON

DEPUTY CHIEF OF STAFF

RESEARCH, DEVELOPMENT, & ACQ

DEPARTMENT OF THE AIR FORCE

WASHINGTON, D.C. 20330

01CY ATTN AFRDQ

HEADQUARTERS

ELECTRONIC SYSTEMS DIVISION

DEPARTMENT OF THE AIR FORCE

HANSCOM AFB, MA 01731

01CY ATTN J. DEAS

HEADQUARTERS

ELECTRONIC SYSTEMS DIVISION/YSEA

DEPARTMENT OF THE AIR FORCE

HANSCOM AFB, MA 01732

01CY ATTN YSEA

HEADQUARTERS

ELECTRONIC SYSTEMS DIVISION/DC

DEPARTMENT OF THE AIR FORCE

HANSCOM AFB, MA 01731

01CY ATTN DCKC MAJ J.C. CLARK

COMMANDER  
FOREIGN TECHNOLOGY DIVISION, AFSC  
WRIGHT-PATTERSON AFB, OH 45433  
O1CY ATTN NICO LIBRARY  
O1CY ATTN ETOP B. BALLARD

COMMANDER  
ROME AIR DEVELOPMENT CENTER, AFSC  
GRIFFISS AFB, NY 13441  
O1CY ATTN DOC LIBRARY/TSLD  
O1CY ATTN OCSE V. COYNE

SAMSO/SZ  
POST OFFICE BOX 92960  
WORLDWAY POSTAL CENTER  
LOS ANGELES, CA 90009  
(SPACE DEFENSE SYSTEMS)  
O1CY ATTN SZJ

STRATEGIC AIR COMMAND/XPFS  
OFFUTT AFB, NB 68113  
O1CY ATTN ADWATE MAJ BRUCE BAUER  
O1CY ATTN NRT  
O1CY ATTN DOK CHIEF SCIENTIST

SAMSO/SK  
P.O. BOX 92960  
WORLDWAY POSTAL CENTER  
LOS ANGELES, CA 90009  
O1CY ATTN SKA (SPACE COMM SYSTEMS)  
M. CLAVIN

SAMSO/MN  
NORTON AFB, CA 92409  
(MINUTEMAN)  
O1CY ATTN MNNL

COMMANDER  
ROME AIR DEVELOPMENT CENTER, AFSC  
HANS COM AFB, MA 01731  
O1CY ATTN EEP A. LORENTZEN

DEPARTMENT OF ENERGY  
LIBRARY ROOM G-042  
WASHINGTON, D.C. 20545  
O1CY ATTN DOC CON FOR A. LABOWITZ

DEPARTMENT OF ENERGY  
ALBUQUERQUE OPERATIONS OFFICE  
P.O. BOX 5400  
ALBUQUERQUE, NM 87115  
O1CY ATTN DOC CON FOR D. SHERWOOD

EG&G, INC.  
LOS ALAMOS DIVISION  
P.O. BOX 809  
LOS ALAMOS, NM 85544  
O1CY ATTN DOC CON FOR J. REEDLOVE

UNIVERSITY OF CALIFORNIA  
LAWRENCE LIVERMORE LABORATORY  
P.O. BOX 308  
LIVERMORE, CA 94550  
O1CY ATTN DOC CON FOR TECH INFO  
DEPT  
O1CY ATTN DOC CON FOR L-389 R. OTT  
O1CY ATTN DOC CON FOR L-31 R. HAGER

LOS ALAMOS NATIONAL LABORATORY  
P.O. BOX 1663  
LOS ALAMOS, NM 87545  
O1CY ATTN DOC CON FOR J. WOLCOTT  
O1CY ATTN DOC CON FOR R.F. TASCHEK  
O1CY ATTN DOC CON FOR E. JONES  
O1CY ATTN DOC CON FOR J. MALIK  
O1CY ATTN DOC CON FOR R. JEFFRIES  
O1CY ATTN DOC CON FOR J. ZINN  
O1CY ATTN DOC CON FOR P. KEATON  
O1CY ATTN DOC CON FOR D. WESTERVELT  
O1CY ATTN D. SAPPENFIELD

SANDIA LABORATORIES  
P.O. BOX 5800  
ALBUQUERQUE, NM 87115  
O1CY ATTN DOC CON FOR W. BROWN  
O1CY ATTN DOC CON FOR A.  
THORNBROUGH  
O1CY ATTN DOC CON FOR T. WRIGHT  
O1CY ATTN DOC CON FOR D. DAHLGREN  
O1CY ATTN DOC CON FOR 3141  
O1CY ATTN DOC CON FOR SPACE PROJECT  
DIV

SANDIA LABORATORIES  
LIVERMORE LABORATORY  
P.O. BOX 969  
LIVERMORE, CA 94550  
O1CY ATTN DOC CON FOR B. MURPHEY  
O1CY ATTN DOC CON FOR T. COOK

OFFICE OF MILITARY APPLICATION  
DEPARTMENT OF ENERGY  
WASHINGTON, D.C. 20545  
O1CY ATTN DOC CON DR. YO SONG

OTHER GOVERNMENT

INSTITUTE FOR TELECOM SCIENCES  
NATIONAL TELECOMMUNICATIONS & INFO  
ADMIN  
BOULDER, CO 80303  
01CY ATTN A. JEAN (UNCLASS ONLY)  
01CY ATTN W. UTLAUT  
01CY ATTN D. CROMBIE  
01CY ATTN L. BERRY

NATIONAL OCEANIC & ATMOSPHERIC ADMIN  
ENVIRONMENTAL RESEARCH LABORATORIES  
DEPARTMENT OF COMMERCE  
BOULDER, CO 80302  
01CY ATTN R. GRUBB  
01CY ATTN AERONOMY LAB G. REID

DEPARTMENT OF DEFENSE CONTRACTORS

AEROSPACE CORPORATION  
P.O. BOX 92957  
LOS ANGELES, CA 90009  
01CY ATTN I. GARFUNKEL  
01CY ATTN T. SALMI  
01CY ATTN V. JOSEPHSON  
01CY ATTN S. BOWER  
01CY ATTN D. OLSEN

ANALYTICAL SYSTEMS ENGINEERING CORP  
5 OLD CONCORD ROAD  
BURLINGTON, MA 01803  
01CY ATTN RADIO SCIENCES

AUSTIN RESEARCH ASSOC., INC.  
1901 RUTLAND DRIVE  
AUSTIN, TX 78758  
01CY ATTN L. SLOAN  
01CY ATTN R. THOMPSON

BERKELEY RESEARCH ASSOCIATES, INC.  
P.O. BOX 983  
BERKELEY, CA 94701  
01CY ATTN J. WORKMAN  
01CY ATTN C. PRETTIE  
01CY ATTN S. BRECHT

BOEING COMPANY, THE  
P.O. BOX 3707  
SEATTLE, WA 98124  
01CY ATTN G. KEISTER  
01CY ATTN D. MURRAY  
01CY ATTN G. HALL  
01CY ATTN J. KENNEY

CHARLES STARK DRAPER LABORATORY, INC.  
555 TECHNOLOGY SQUARE  
CAMBRIDGE, MA 02139  
01CY ATTN D.B. COX  
01CY ATTN J.P. GILMORE

COMSAT LABORATORIES  
LINTHICUM ROAD  
CLARKSBURG, MD 20734  
01CY ATTN G. HYDE

CORNELL UNIVERSITY  
DEPARTMENT OF ELECTRICAL ENGINEERING  
ITHACA, NY 14850  
01CY ATTN D.T. FARLEY, JR.

ELECTROSPACE SYSTEMS, INC.  
BOX 1359  
RICHARDSON, TX 75080  
01CY ATTN H. LOGSTON  
01CY ATTN SECURITY (PAUL PHILLIPS)

EOS TECHNOLOGIES, INC.  
606 Wilshire Blvd.  
Santa Monica, Calif 90401  
01CY ATTN C.B. GABBARD  
01CY ATTN R. LELEVIER

ESL, INC.  
495 JAVA DRIVE  
SUNNYVALE, CA 94086  
01CY ATTN J. ROBERTS  
01CY ATTN JAMES MARSHALL

GENERAL ELECTRIC COMPANY  
SPACE DIVISION  
VALLEY FORGE SPACE CENTER  
GODDARD BLVD KING OF PRUSSIA  
P.O. BOX 8555  
PHILADELPHIA, PA 19101  
01CY ATTN M.H. BORTNER  
SPACE SCI LAB

GENERAL ELECTRIC COMPANY  
P.O. BOX 1122  
SYRACUSE, NY 13201  
01CY ATTN F. REIBERT

GENERAL ELECTRIC TECH SERVICES  
CO., INC.  
HMES  
COURT STREET  
SYRACUSE, NY 13201  
01CY ATTN G. MILLMAN

GEOPHYSICAL INSTITUTE  
UNIVERSITY OF ALASKA  
FAIRBANKS, AK 99701  
(ALL CLASS ATTN: SECURITY OFFICER)  
01CY ATTN T.N. DAVIS (UNCLASS ONLY)  
01CY ATTN TECHNICAL LIBRARY  
01CY ATTN NEAL BROWN (UNCLASS ONLY)

GTE SYLVANIA, INC.  
ELECTRONICS SYSTEMS GRP-EASTERN DIV  
77 A STREET  
NEEDHAM, MA 02194  
01CY ATTN DICK STEINHOF

HSS, INC.  
2 ALFRED CIRCLE  
BEDFORD, MA 01730  
01CY ATTN DONALD HANSEN

ILLINOIS, UNIVERSITY OF  
107 COBLE HALL  
150 DAVENPORT HOUSE  
CHAMPAIGN, IL 61820  
(ALL CORRES ATTN DAN MCCLELLAND)  
01CY ATTN K. YEH

INSTITUTE FOR DEFENSE ANALYSES  
1301 NO. BEAUREGARD STREET  
ALEXANDRIA, VA 22311  
01CY ATTN J.M. AEIN  
01CY ATTN ERNEST SAUER  
01CY ATTN HANS WOLFARD  
01CY ATTN JOEL BENGSTON

INTL TEL & TELEGRAPH CORPORATION  
500 WASHINGTON AVENUE  
NUTLEY, NJ 07110  
01CY ATTN TECHNICAL LIBRARY

JAYCOR  
11011 TORREYANA ROAD  
P.O. BOX 85154  
SAN DIEGO, CA 92138  
01CY ATTN J.L. SPERLING

JOHNS HOPKINS UNIVERSITY  
APPLIED PHYSICS LABORATORY  
JOHNS HOPKINS ROAD  
LAUREL, MD 20810  
01CY ATTN DOCUMENT LIBRARIAN  
01CY ATTN THOMAS POTEIRA  
01CY ATTN JOHN DASSOULAS

KAMAN SCIENCES CORP  
P.O. BOX 7463  
COLORADO SPRINGS, CO 80933  
01CY ATTN T. MEAGHER

KAMAN TEMPO-CENTER FOR ADVANCED  
STUDIES  
816 STATE STREET (P.O. DRAWER 99)  
SANTA BARBARA, CA 93102  
01CY ATTN DASIAE  
01CY ATTN WARREN S. KNAPP  
01CY ATTN WILLIAM MCNAMARA  
01CY ATTN B. GAMBILL

LINKABIT CORP  
10453 ROSELLE  
SAN DIEGO, CA 92121  
01CY ATTN IRWIN JACOBS

LOCKHEED MISSILES & SPACE CO., INC  
P.O. BOX 504  
SUNNYVALE, CA 94088  
01CY ATTN DEPT 60-12  
01CY ATTN D.R. CHURCHILL

LOCKHEED MISSILES & SPACE CO., INC.  
3251 HANOVER STREET  
PALO ALTO, CA 94304  
01CY ATTN MARTIN WALT DEPT 52-12  
01CY ATTN W.L. IMHOF DEPT 52-12  
01CY ATTN RICHARD G. JOHNSON  
DEPT 52-12  
01CY ATTN J.B. CLADIS DEPT 52-12

MARTIN MARIETTA CORP  
ORLANDO DIVISION  
P.O. BOX 5837  
ORLANDO, FL 32805  
01CY ATTN R. HEFFNER

M.I.T. LINCOLN LABORATORY  
P.O. BOX 73  
LEXINGTON, MA 02173  
01CY ATTN DAVID M. TOWLE  
01CY ATTN L. LOUGHLIN  
01CY ATTN D. CLARK

MCDONNELL DOUGLAS CORPORATION  
5301 BOLSA AVENUE  
HUNTINGTON BEACH, CA 92647

01CY ATTN W. HARRIS  
01CY ATTN J. MOBLE  
01CY ATTN GEORGE WROE  
01CY ATTN W. OLSON  
01CY ATTN R.W. HALPRIN  
01CY ATTN TECHNICAL  
LIBRARY SERVICES

MISSION RESEARCH CORPORATION  
735 STATE STREET  
SANTA BARBARA, CA 93101

01CY ATTN P. FISCHER  
01CY ATTN W.F. CREVIER  
01CY ATTN STEVEN L. GUTSCHE  
01CY ATTN R. BOGUSCH  
01CY ATTN R. HENDRICK  
01CY ATTN RALPH KILB  
01CY ATTN DAVE SOWLE  
01CY ATTN F. FAJEN  
01CY ATTN M. SCHEIBE  
01CY ATTN CONRAD L. LONGMIRE  
01CY ATTN B. WHITE  
01CY ATTN R. STAGAT

MISSION RESEARCH CORP.  
1720 RANDOLPH ROAD, S.E.  
ALBUQUERQUE, NEW MEXICO 87106

01CY R. STELLINGWERF  
01CY M. ALME  
01CY L. WRIGHT

MITRE CORPORATION, THE  
P.O. BOX 208

BEDFORD, MA 01730  
01CY ATTN JOHN MORGANSTERN  
01CY ATTN G. HARDING  
01CY ATTN C.E. CALLAHAN

MITRE CORP  
WESTGATE RESEARCH PARK  
1320 DOLLY MADISON BLVD  
MCLEAN, VA 22101

01CY ATTN W. HALL  
01CY ATTN W. FOSTER

PACIFIC-SIERRA RESEARCH CORP  
12340 SANTA MONICA BLVD.  
LOS ANGELES, CA 90025

01CY ATTN E.C. FIELD, JR.

PENNSYLVANIA STATE UNIVERSITY  
IONOSPHERE RESEARCH LAB  
318 ELECTRICAL ENGINEERING EAST  
UNIVERSITY PARK, PA 16802  
(NO CLASS TO THIS ADDRESS)  
01CY ATTN IONOSPHERIC RESEARCH LAB

PHOTOMETRICS, INC.  
4 ARROW DRIVE  
WOBURN, MA 01801  
01CY ATTN IRVING L. KOFISKY

PHYSICAL DYNAMICS, INC.  
P.O. BOX 3027  
BELLEVUE, WA 98009  
01CY ATTN E.J. FREMOUW

PHYSICAL DYNAMICS, INC.  
P.O. BOX 10367  
OAKLAND, CA 94610  
ATTN A. THOMSON

R & D ASSOCIATES  
P.O. BOX 9695  
MARINA DEL REY, CA 90291  
01CY ATTN FORREST GILMORE  
01CY ATTN WILLIAM B. WRIGHT, JR.  
01CY ATTN WILLIAM J. KARZAS  
01CY ATTN H. ORY  
01CY ATTN C. MACDONALD  
01CY ATTN R. TURCO  
01CY ATTN L. DERAND  
01CY ATTN W. TSAI

RAND CORPORATION, THE  
1700 MAIN STREET  
SANTA MONICA, CA 90406  
01CY ATTN CULLEN CRAIN  
01CY ATTN ED REDROZIAN

RAYTHEON CO.  
528 BOSTON POST ROAD  
SUDBURY, MA 01776  
01CY ATTN BARBARA ADAMS

RIVERSIDE RESEARCH INSTITUTE  
330 WEST 42nd STREET  
NEW YORK, NY 10036  
01CY ATTN VINCE TRAPANI



SCIENCE APPLICATIONS, INC.  
1150 PROSPECT PLAZA  
LA JOLLA, CA 92037

01CY ATTN LEWIS M. LINSON  
01CY ATTN DANIEL A. HAMLIN  
01CY ATTN E. FRIEMAN  
01CY ATTN E.A. STRAKER  
01CY ATTN CURTIS A. SMITH

SCIENCE APPLICATIONS, INC  
1710 GOODRIDGE DR.  
MCLEAN, VA 22102

01CY J. COCKAYNE  
01CY E. HYMAN

SRI INTERNATIONAL  
333 PAVENSWOOD AVENUE  
MENLO PARK, CA 94025

01CY ATTN J. CASPER  
01CY ATTN DONALD NEILSON  
01CY ATTN ALAN BURNS  
01CY ATTN G. SMITH  
01CY ATTN R. TSUNODA  
01CY ATTN DAVID A. JOHNSON  
01CY ATTN WALTER G. CHESNUT  
01CY ATTN CHARLES L. RINO  
01CY ATTN WALTER JAYE  
01CY ATTN J. VICKREY  
01CY ATTN RAY L. LEADABRAND  
01CY ATTN G. CARPENTER  
01CY ATTN G. PRICE  
01CY ATTN R. LIVINGSTON  
01CY ATTN V. GONZALES  
01CY ATTN D. MCDANIEL

TECHNOLOGY INTERNATIONAL CORP  
75 WIGGINS AVENUE  
BEDFORD, MA 01730  
01CY ATTN W.P. BOQUIST

TOYON RESEARCH CO.  
P.O. Box 6890  
SANTA BARBARA, CA 93111  
01CY ATTN JOHN ISE, JR.  
01CY ATTN JOEL GARBARINO

TRW DEFENSE & SPACE SYS GROUP  
ONE SPACE PARK

REDONDO BEACH, CA 90278  
01CY ATTN R. K. PLESUCH  
01CY ATTN S. ALTSCHULER  
01CY ATTN D. DEE  
01CY ATTN D/ STOCKWELL  
SNTF/1575

VISIDYNE  
SOUTH BEDFORD STREET  
BURLINGTON, MASS 01803  
01CY ATTN W. REIDY  
01CY ATTN J. CARPENTER  
01CY ATTN C. HUMPHREY

UNIVERSITY OF PITTSBURGH  
PITTSBURGH, PA 15213  
01CY ATTN: N. ZARUSKY

DIRECTOR OF RESEARCH  
U.S. NAVAL ACADEMY  
ANNAPOLIS, MD 21402  
02CY

**END**

**FILMED**

**8-85**

**DTIC**